Mac/Lac-tosylceramide regulates intestinal homeostasis and secretory cell fate commitment by facilitating Notch signaling

Kebei Tang[1, 2#], Xuewen Li[1#], Jiulong Hu[1, 3#], Jingyuan Shi[1], Yumei Li[1], Yansu Chen[1], Chang Yin[1], Fengchao Wang[1, 4], and Rongwen Xi[1, 4*]

[1] National Institute of Biological Sciences, No. 7 Science Park Road, Zhongguancun Life Science Park, Beijing 102206, China

[2] Academy for Advanced Interdisciplinary Studies, Peking University, Beijing 100871, China

[3] School of Life Sciences, Tsinghua University, Beijing 100084, China

[4] Tsinghua Institute of Multidisciplinary Biomedical Research, Tsinghua University, Beijing 102206, China.

[#] These authors contributed equally to this work.

* Correspondence: *xirongwen@nibs.ac.cn*

Abstract

Cell-to-cell communication via Delta-Notch signaling is widely used in various tissues and organs to regulate development and patterning; however, the mechanisms regulating Notch signaling for precise cell fate decisions remain poorly understood. Similar to mammals, the intestinal stem cells (ISCs) in the adult *Drosophila* midgut generate both absorptive and secretory cell progeny, guided by differential levels of Notch activation. Here we performed a forward genetic screen in *Drosophila* and identified glucosylceramide synthase (GlcT), a rate-limiting enzyme for glycosphingolipid (GSL) production, whose mutation causes the development of secretory cell tumors. Genetic analysis of the GSL synthesis pathway, combined with metabolite rescue experiments, revealed that the tumor formation is linked to a deficiency in Mactosylceramide/Lactosylceramide. This deficiency impaired the endocytic recycling of the Delta, subsequently reducing Notch signaling activation. Conditional knockout of *UGCG*, the mammalian ortholog of *GlcT*, in mouse small intestine caused an excessive differentiation of goblet cells, phenotypes similar to these caused by Notch inhibition. Our study suggests an evolutionarily conserved role for a specific GSL metabolite in modulating Notch signaling during stem cell fate decisions and provides a molecular connection between ceramide metabolism and Notch signaling in regulating tissue homeostasis and tumor formation.

INTRODUCTION

Notch signaling is an evolutionarily conserved pathway in metazoans that mediates local cell-cell interactions through the membrane-tethered ligand Delta (Dl) and the membrane receptor Notch. This pathway transduces signals from the cell surface to the nucleus, regulating the transcription of target genes [1,2]. Dl-Notch signaling controls various cell fates and developmental processes, with mutations in the pathway implicated in numerous human diseases, including congenital defects and cancer [3-5]. Given that Notch can transduce, amplify, and consolidate molecular differences to influence cell fate decisions, it is crucial to understand how the strength of the Notch signaling pathway is precisely regulated to ensure proper cell fate determination and tissue development.

Notch signaling is known as a major regulator of cell fate decisions in both mammalian and *Drosophila* intestinal stem cell (ISC) lineages, as its activity determines the binary fate of intestinal progenitor cells. A high level of Notch activity promotes the specification of absorptive enterocytes, while low or absent Notch activity favors the specification of secretory cell types.[6,7]. The *Drosophila* intestinal stem cell (ISC) lineage in the adult midgut is relatively simple, comprising only one type of secretory cell: enteroendocrine cells (EEs). This simplicity makes it an attractive experimental system for studying Notch signaling in cell fate decisions during epithelial renewal [6]. The fly ISCs, which specifically express Dl, periodically generate two types of committed daughter cells: enteroblasts, which experience high levels of Notch activation and are primed for the specification of absorptive enterocytes, and enteroendocrine progenitor cells (EEPs), which receive low levels of Notch activation. Typically, EEPs undergo one round of mitosis before terminal differentiation, resulting in the formation of EE pairs [8-11]. The loss of Notch signaling results in a complete blockage of enteroblast differentiation, leading to the accumulation of ISCs, EEPs and EEs in the intestinal epithelium, producing an "EE tumor" phenotype [8,10]. It is suggested that the expression level of Dl in individual ISCs varies, leading to differential levels of Notch activation in the immediate daughter cells [9]. This variation in Dl expression may result from dynamic bidirectional Dl-Notch signaling between ISCs and EEPs, which in parallel or in conjunction with an intrinsic feedback mechanism in ISCs,

66 guides a periodic activation of an EE fate inducer Scute, thereby periodic generation of EEPs
67 from ISCs [10,12,13]. The transient activation of Scute induces irreversible Prospero expression in
68 EEPs through a Phyl-Sina-Ttk69 regulatory cascade, initiating terminal differentiation into EEs
69 [10,14-16]. During the period of Scute inactivation, ISCs only generate enterocyte-committed
70 enterobalsts by default via Dl-Notch mediated lateral inhibition [8,17]. In newly enclosed flies,
71 increased lipid intake from food can alter the membrane trafficking of Dl, subsequently
72 increasing the frequency of EE specification from ISCs [18]. Thus, both intrinsic and extrinsic
73 mechanisms are involved in regulating Dl-Notch signaling to orchestrate stem cell fate
74 decisions.

75

76 To better understand fate regulation in the *Drosophila* ISC lineage, here we conducted a
77 forward mosaic genetic screen in the adult *Drosophila* midgut, focusing on the right arm of the
78 second chromosome to identify genes whose mutations could disrupt ISC fate decisions. From
79 this screen, we identified several complementation groups that result in EE tumor phenotypes.
80 While most of the identified gene loci correspond to known components of the Notch signaling
81 pathway, we discovered one gene locus not previously associated with Notch signaling.
82 Further analyses revealed a specific GSL metabolite that regulates Notch signaling and cell fate
83 decisions in the intestinal epithelium, and this function appears to be conserved from
84 *Drosophila* to mice.

85

86 **RESULTS**

87 **A mosaic genetic screen identifies *GlcT* as a tumor suppressor in the adult *Drosophila* midgut**

88 We performed EMS mutagenesis on chromosome 2R (carrying FRTG13/42B, 12 and used the
89 MARCM system to induce mutant clones in the adult midgut (Supplementary Figure 1). We
90 screened approximately 10,000 lethal lines and identified totally 12 mutations across six
91 complementation groups that exhibited a "small cell tumor" phenotype, characterized by a
92 significant accumulation of diploid cells within the clones (Supplementary Figure 1 and
93 supplementary Table 1). Co-staining with the ISC marker Dl and the EE cell marker Pros

94 revealed that most of these tumors contained an excessive number of ISCs and EEs, the EE
95 tumor phenotype commonly observed in Notch mutant clones [11,19]. Further genetic mapping
96 showed that three complementation groups were associated with genes known to function in
97 the Notch pathway: *mam*, *Gmer*, and *O-fut1* [20-22]. One complementation group, comprising
98 two alleles (*EA30* and *E230*), mapped to the *GlcT* gene (see details in Methods), while the
99 remaining two complementation groups, each consisting of one allele, remain undetermined
100 (Supplementary Table 1). *GlcT* encodes glucosylceramide synthase, an enzyme that catalyzes
101 the formation of glucosylceramide, the core component of glycosphingolipids (GSLs). Both
102 alleles carried one or more missense mutations resulting in the amino acid replacements
103 E292K (for *EA30*) and L395P/S397T (for *E230*, Figure S1D). The two mutations produced a
104 similar tumor phenotype in terms of tumor size and the composition of EEs in the tumors
105 (Figure 1B-D). The large polyploid cells were still present in the tumors, indicating that the
106 multipotency of ISCs was retained, but the differentiation of ISCs may have been biased
107 towards the EE fate commitment. Additionally, $GlcT^{\Delta 8}$, a previously characterized null allele of
108 *GlcT* [23], exhibited a similar EE tumor phenotype (Figure 1B-D). Expressing a *UAS-GlcT* transgene
109 in the mutant clones fully prevented the tumor phenotype (Figure 1E, F). Furthermore,
110 depleting *GlcT* in progenitor cells using RNAi with $esg\text{-}GAL4^{ts}$ also led to overproliferation of
111 ISCs and excessive generation of EEs in the midgut epithelium (Figure 1G-I). Taken together,
112 these data suggest that *GlcT* acts as a tumor suppressor in adult *Drosophila* midgut. Loss of
113 *GlcT* induces ISC over-proliferation and excessive EE differentiation, resulting in an EE tumor
114 or "neuroendocrine tumor (NET)" phenotype.

115

116 **Genetic analysis of the GSL synthesis pathway components reveals specific tumor-**
117 **suppressive activity for *egh*, in addition to *GlcT***

118 GlcT is involved in the initial step in the GSL biosynthesis pathway, which synthesizes
119 glucosylceramide by transferring glucose to ceramide (Figure 2A). The loss of *GlcT* could result
120 in the accumulation of ceramide or the absence of glucosylceramide and the downstream GSL
121 metabolites. Ceramide accumulation has been linked to promoting cell apoptosis [24], which
122 could potentially explain the ISC over-proliferation phenotype since apoptotic cells can induce

123 compensatory ISC proliferation [25]. However, we did not observe a significant increase in
124 apoptotic cells within the mutant clones (Figure 2B). Moreover, the overexpression of p35, an
125 inhibitor of cell apoptosis, failed to suppress or alleviate the tumor phenotype (Figure 2B).
126 Ceramidase (CDase) catalyzes ceramide into shingosine and free fatty acid, and overexpressing
127 *CDase* can in theory downregulate ceramide levels. We therefore introduced *CDase* expression
128 in the mutant clones, but this intervention also did not alleviate the tumor phenotype (Figure
129 2B). Hence, the EE tumors developed from *GlcT* mutant clones is unlikely caused by the
130 accumulation of ceramide.

131

132 In the GSL biosynthesis pathway in *Drosophila*, glucosylceramide undergoes sequential
133 modifications catalyzed by Egghead (Egh) and Brainiac (Brn), which add the second (Mactosyl-)
134 and third (GlcNAc-) glycosyl residues, respectively (Figure 2A) [26,27]. This leads to the synthesis
135 of Mactosylceramide (MacCer) and GlcNAcβ1-3Manβ1-4Glcβ1Ceramide. Complex GSL
136 biosynthesis involves the participation of β4-N-Acetylgalactosyltransferase (*β4GalNAcTA/TB*)
137 and α1,4-Galactosyltransferase (*α4GT1/2*) in the fourth and fifth steps of GSL sugar chain
138 elongation [28,29]. These enzymes catalyze the formation of GalNAcβ1-4GlcNAcβ1-3Manβ1-
139 4Glcβ1Ceramide and GalNAc-α1-4GalNAcβ1-4GlcNAcβ1-3Manβ1-4Glcβ1Ceramide,
140 respectively.

141

142 To understand the consequences of mutations in these GSL biosynthesis pathway genes, we
143 generated mutant MARCM clones for each of the above-mentioned genes and examined their
144 effects. Interestingly, mutations in *egh*, assessed using three different loss-of-function alleles,
145 consistently resulted in cell over-proliferation and excessive EE phenotypes, similar to those
146 caused by the loss of *GlcT* (Figure 2E-G). In contrast, none of the mutant clones of *brn*,
147 *β4GalNAcTA*, or *α4GT1* exhibited any noticeable abnormalities in clone size or percentages of
148 EEs, when compared to the control group of wild-type clones (Figure 2E-G). Therefore, GlcT
149 and Egh, but not other enzymes in the GSL biosynthesis pathway, exhibit specific tumor
150 suppressive activity in the adult *Drosophila* midgut.

151

152 **The EEC tumor phenotype is a result of MacCer deficiency**

153 As Egh is necessary for the biosynthesis of MacCer, the specific phenotype resulted from the
154 loss GlcT and Egh but not Brn could be attributed to the absence of MacCer. To test this
155 hypothesis, we fed flies carrying *GlcT* mutant clones with Lactosylceramide (LacCer), an analog
156 of MacCer that functions similarly to MacCer in mammalian cells. Remarkably, LacCer
157 significantly suppressed the overgrowth and excessive EE phenotype in the anterior midgut
158 clones (Figure 3). The suppression effect was also significant, though relatively mild, in the
159 posterior midgut (Figure 3). This difference may be attributed to substantial absorption or
160 metabolism of LacCer prior to its entry into the posterior midgut. Therefore, among the
161 various GSL metabolites, MacCer and LacCer appear to possess specific tumor-suppressive
162 activities in the *Drosophila* midgut.

163

164 **Loss of *GlcT* leads to reduced activation of Notch signaling in ISC progenies.**

165 In adult *Drosophila* midgut, the proliferation and differentiation of ISCs are regulated by
166 multiple signaling pathways. Among these, the EGFR/Ras/MAPK and JAK/STAT signaling
167 pathways play significant roles in promoting ISC proliferation during intestinal renewal and
168 regeneration following tissue damage or infection [30,31]. Additionally, Notch signaling not only
169 regulates ISC proliferation but also controls fate decisions between EE/EC during ISC
170 differentiation [19,32,33]. Loss of Notch leads to increased ISC proliferation and excessive EE
171 generation, phenotype similar to those caused by *GlcT* mutations. Therefore, we examined
172 whether the loss of *GlcT* affects the activities of these signaling pathways.

173

174 Normally, among the intestinal cells in the midgut epithelium, progenitor cells including ISCs
175 and enteroblasts, exhibit low but specific activation of EGFR and JAK/STAT activities [30,31,34]. The
176 growth of *GlcT* mutant clones appeared to cause a general increase of EGFR and JAK/STAT
177 activities within the intestinal epithelium, as many differentiated cells also exhibited EGFR or

178 JAK/STAT signaling activation (Supplementary Figure 2), which is likely due to stress responses
179 induced by tumor growth [35]. Nevertheless, we observed that pERK, a direct indicator of
180 EGFR/Ras/MAPK signaling activity, was not significantly increased in *GlcT* mutant cells
181 compared to cells outside the clones (Supplementary Figure 2). Similarly, the nuclear
182 expression of STAT92E, which reflects JAK/STAT pathway activation, did not show significant
183 changes in *GlcT* mutant cells compared to normal cells outside the clones (Supplementary
184 Figure 2). However, the expression of *NRE-lacZ*, a reporter for Notch pathway activation, was
185 specifically down-regulated in *GlcT* mutant clones. Most cells within the clones exhibited lower
186 LacZ expression levels compared to *NRE-lacZ* positive cells outside the clones (Figure 4A, B).
187 Previous studies have shown that while the loss of function of Notch completely blocks EC
188 differentiation from ISCs, a reduction in Notch activity does not necessarily hinder EC
189 differentiation from ISCs. Instead, it may lead to a dose-dependent increase in the ratio of
190 differentiated EEs to ECs, depending on the severity of Notch loss [19]. Therefore, the increased
191 EE to EC ratio and the reduced NRE-lacZ expression observed in *GlcT* mutant clones collectively
192 suggest that the mutant phenotype may be caused by a reduction in Notch signaling activity.

193

194 In the ISC lineage, Notch signaling not only guides EC/EE fate decisions, but is also participated
195 in regulating EE subtype diversity. Typically, each EEP undergo one round of asymmetric cell
196 division to yield a pair of distinctive EEs, an allatostatin C $(AstC)^+$ class I EE and a tachykinin
197 $(Tk)^+$ class II EE [10]. The loss of *Notch* specifically compromises Mirr-dependent specification of
198 class II EE generation, resulting in all EEs in *Notch* mutant clones becoming $AstC^+$ class I EEs
199 [16,36]. We found that in *GlcT* mutant clones, virtually all EEs were positive for AstC but TK (Figure
200 4C), further supporting the idea that Notch signaling is compromised in these clones.

201

202 We next tested whether forced activation of Notch in *GlcT* mutant clones could suppress the
203 EE tumor phenotype. To achieve this, we expressed N^{intra}, an active form of Notch, in *GlcT*
204 mutant clones. As expected, this resulted in the complete suppression of cell proliferation in
205 *GlcT* mutant clones and promoted the differentiation of these cells into ECs, leading all clones

206 to become single-cell clones that often contained a polyploid cell (Figure 4D). This finding
207 suggests that N^{intra} is epistatic to *GlcT* in the signaling transduction pathway, indicating that
208 GlcT may regulate Notch signaling at the ligand/receptor level.

209

210 ***GlcT* regulates the endocytic trafficking of Delta.**

211 The observations above collectively suggest that full activation of Notch signaling in the ISC
212 lineage may require a specific GSL: Mac/Lac-Cer. As transmembrane proteins, the proper
213 internalization and recycling of Dl and Notch are important for the proper activation of Notch
214 signaling [37,38]. Specific lipids have been implicated in the formation of micro-domains on the
215 cell membrane, which play a role in regulating cell-cell signaling [39]. Therefore, we asked
216 whether the loss of MacCer caused by *GlcT* mutation could disrupt Notch signaling by affecting
217 the stability, endocytosis, or recycling of either Dl or Notch.

218

219 Knocking down *GlcT* in ISCs using *Dl-GAL4*^{ts} cased an increase in EEs in the midgut epithelium
220 (Figure 5 A, B). However, when *GlcT* was specifically knocked down in EBs using *NRE-GAL4*^{ts},
221 there was no noticeable increase in EEs (Figure 5 A, B). This indicates that GlcT is probably
222 required in ISCs and implies its potential role on the regulation of Dl. However, the lack of an
223 observable phenotype using NRE-Gal4 could be due to delayed expression, which may result
224 in missing the critical window required for effective *GlcT* knockdown. Consequently, we cannot
225 rule out the possibility that GlcT also plays a role in early EBs or EEPs.

226

227 It is well-known that the internalization of Dl in the signaling-sending cell is necessary for
228 Notch activation in the signaling-receiving cell [37]. To investigate whether the endocytosis
229 process of Dl is altered in *GlcT* mutant ISCs, we performed an *ex vivo* Dl internalization assay,
230 following the previously described protocol [40]. In this assay, we cultured and incubated the
231 freshly dissected gut with anti-Dl antibodies, and the endocytosis of the antibody-labeled Dl
232 was visualized after fixation and immunostaining with secondary antibodies. Interestingly,

233 during the 3-hour period, we observed a significant difference in the subcellular localization
234 pattern of Dl between normal and *GlcT* mutant ISCs (Figure 5 C, D). In *GlcT* mutant ISCs, the
235 majority of labeled Dl had already been internalized, while in wild-type ISCs, it remained on
236 the cell membrane. This observation suggests that the loss of *GlcT* causes either reduced
237 stability of Dl on the cell membrane or accelerated internalization of Dl from the cell
238 membrane.

239

240 To further characterize the endocytic trafficking of Dl in *GlcT* mutant ISCs, we performed
241 conditional depletion of *GlcT* and examined the co-localization of internalized Dl with the early
242 endosome marker Rab5, the late endosome marker Rab7, and the recycle endosome marker
243 Rab11, respectively. In comparison to control ISCs, *GlcT-IR* ISCs exhibited a significant increase
244 in early endosomes containing Dl (Figure 5E, F). However, the percentage of late and recycle
245 endosomes containing Dl remained similar between wild-type and *GlcT-IR* ISCs (Figure 5E, F).
246 These observations suggest that the internalized Dl in *GlcT-IR* ISCs experiences a delay in early
247 endosomes, which might cause a delay in Dl recycling and consequently a reduction in Dl-
248 Notch signaling activity (Figure 7E).

249

250 ***GlcT* shows tissue specificity in regulating Notch signaling activity**

251 Notch signaling has pleiotropic function and is known to be participated in the development
252 of diverse tissue and organs. We therefore asked whether the discovered mechanism above is
253 generally utilized in controlling Notch signaling in diverse tissues and organs. In the wing disc
254 of third instar larvae, Notch signaling is activated by ligands Dl and Serrate at the dorsal-ventral
255 boundary to induce the expression of Cut [41]. We found that in *GlcT* mutant clones spanning
256 the dorsal-ventral boundary region of the wing disc, the expression of Cut was not significantly
257 altered (Figure 6A). This indicates that *GlcT* is not essential for regulating Notch-mediated Cut
258 expression in this specific context.

259

260 During oogenesis in the *Drosophila* ovary, Notch signaling regulates differentiation and
261 transition of follicle cells from the mitotic cell cycle to the endocycle during stage 6 [42,43]. We
262 found that in the developing egg chambers with germline mutations of *GlcT*, the patterning of
263 the surrounding follicle cells remained largely normal (Figure 6B). However, we observed an
264 abnormal accumulation of Dl protein in cytoplasmic vesicles of the mutant germline cells
265 (Figure 6C), indicating that there is a defect in Dl trafficking in *GlcT* mutant germline cells.
266 However, this defect is not sufficient to impact Dl-Notch signaling to a degree where follicle
267 cell development is adversely affected. Collectively, these observations suggest that the role
268 for GlcT in Notch signaling does not appear to be a universal mechanism across all
269 developmental contexts. Even in situations where this mechanism is involved, the extent to
270 which GlcT affects Dl-Notch signaling may vary in different developmental scenarios.

271

272 **Transient loss of *UGCG* in mouse small intestine causes reduced number of ISCs and**
273 **increased number of goblet cells**

274 As both the Notch signaling and the metabolic pathway of GSLs are conserved from *Drosophila*
275 to mammals, we asked whether this mechanism is conserved in the mouse small intestine to
276 regulate the proliferation and differentiation of ISCs. Notch is known to control the absorptive
277 versus secretory cell fate of mammalian intestinal progenitors as well, and the inhibition of
278 Notch signaling in the intestinal epithelium of mouse small intestine leads excessive number
279 of goblet cells [44,45]. However, unlike in *Drosophila*, Notch positively regulates ISC self-renewal
280 in mice. The inhibition of Notch causes ISC loss, and the excessive activation of Notch promotes
281 the proliferation of intestinal progenitor cells [45,46]. We therefore performed conditional
282 knockout of *UGCG*, which encodes the mammalian glucosylceramide synthase, in the mouse
283 small intestine and examined the consequences.

284

285 It has been previously reported that in the new born mice with intestine-specific knockout of
286 *UGCG*, the proliferation of enterocytes appeared largely normal. However, 3-4 days after
287 intestinal-specific knockout of UGCG in adult mice, epithelial phenotypes including epithelial

288 hyperproliferation, impaired lipid absorption and the detachment of enterocytes from the
289 basal lamina were observed, and these phenotypes are considered to be consequences of gut
290 barrier disruption [47]. To separate the primary from the secondary phenotypes, we repeated
291 the experiment by generating *UGCG*$^{flox/flox}$*; Vil-CreERT2* mice, and examined the phenotype at
292 48h post tamoxifen administration, an early timepoint with a hope that the secondary
293 phenotypes have not yet developed.

294

295 Consistent with the previous findings, the conditional knockout mice showed a severe diarrhea
296 phenotype and died several days following tamoxifen induction. Interestingly, we observed a
297 few phenotypes at the 48h timepoint that was not observed before. We found that in the
298 mutant intestine, there was a marked increase in crypt depth accompanied by a marked
299 reduction in villus length (Supplementary Figure 3). In addition, an excess population of goblet
300 cells was observed, dispersed along the crypt-villus axis (Figure 7C, D). By examining the
301 expression of Olfm4, which is transcriptionally regulated by Notch in ISCs [48], we found that the
302 fluorescence intensity of Olfm4 staining was significantly reduced in *UGCG* mutant ISCs (Figure
303 7A, B). It is unclear how the crypt-villus morphology phenotype is developed in *UGCG* mutant
304 epithelium, but the increased goblet cells and the reduced expression level of Olfm4 are
305 consistent with a Notch phenotype, suggesting a conserved role for glucosylceramide synthase
306 in modulating Notch signaling from *Drosophila* to mammals.

307

308 **Discussion**

309 From an unbiased genetic screen on the right arm of chromosome II, here we have pinpointed
310 four mutant loci that cause an excessive EE phenotype in the intestinal epithelium. Three of
311 them encode known components of the Notch signaling (*mam*, *Gmer*, and *O-fut1*), and the
312 remaining one, *GlcT*, turns out to be a new Notch regulator as well. This work further
313 reinforces the notion that Notch as the key regulator of the secretory versus absorptive cell
314 fate decisions from ISCs, and reveals an evolutionarily conserved link between GSL metabolism
315 and Notch signaling in regulating intestinal homeostasis.

316

317 As *GlcT* encodes glucosylceramide synthase, which that catalyzes the formation of
318 glucosylceramide from ceramide, we further analyzed *egh* and *brn*, which encodes enzymes
319 for the subsequent sequential modifications of glucosylceramide by adding the second
320 (Mactosyl-) and third (GlcNAc-) glycosyl residues, respectively. We found that loss of *egh*, but
321 not *brn*, can give rise to a similar excessive EE phenotype. In addition, the phenotype caused
322 by *GlcT* can be suppressed by feeding with LacCer, which is analogous to MacCer. Collectively,
323 these observations demonstrate that the excessive EE phenotype caused by *GlcT* or *egh*
324 mutation is a result of MacCer deficiency.

325

326 GSLs constitute a specific category of glycolipids localized on the outer leaflet of eukaryotic
327 cell membranes, and studies have implicated their roles in regulating multiple cellular signaling
328 pathways by serving on the lipid raft to facilitate signaling transductions [49-52]. In particular,
329 there is an evolutionarily conserved phospholipid binding domain (C2 domain) on the Notch
330 ligand that is known to interacts with GSLs, and this interaction facilitates ligand-receptor
331 interactions and thereby promotes robust Notch signaling [53-55]. Our analyses of *GlcT* mutant
332 cells in the *Drosophila* midgut suggest that MacCer may represent a key member of GSLs in
333 facilitating Dl-Notch signaling transduction between intestinal stem cells (ISCs) and their
334 immediate progeny to steer binary cell fate decisions. To do so, MacCer may help to modulate
335 the endocytic trafficking of Dl, an event that is known to be essential for Notch activation. We
336 found that Dl on membrane of *GlcT* mutant ISCs tends be rapidly endocytosed and the
337 resultant endosomes appear to experience a delay in transition from early endosome to late
338 endosome. Prior genetic investigations have linked glycosphingolipids synthesized by α4GT1
339 to the modulation of Dl ligand activity i*n vivo*. While the loss of α4GT1 does not overtly affect
340 Dl-Notch signaling, it can exacerbate the wing phenotype of haploinsufficient *Notch* mutants.
341 Furthermore, the overexpression of α4GT1 has been shown to counteract signaling and
342 endocytosis dysfunctions of Dl caused by the inhibition of the E3 ligase Mib1 or Neur activity
343 [50]. Therefore, the robust genetic results presented in this study provide definitive evidence for
344 a functional role of MacCer and its downstream derivatives in regulating Notch signaling.

345 Future structural studies focusing on the interactions between GSLs and Dl should offer
346 valuable insights into the role of GSLs in modulating Dl-Notch interactions and membrane
347 trafficking processes.

348

349 One intriguing observation from our study is the tissue-specific regulatory role of *GlcT* in Notch
350 signaling. Its loss in ISCs significantly impairs Notch signaling, leading to the formation of EE
351 tumors. However, when *GlcT* is lost in the germline cyst within the developing egg chamber, it
352 only modestly disrupts the endocytic trafficking of Dl, without conspicuous effects on the
353 differentiation and patterning of surrounding follicle cells. In the context of imaginal discs, the
354 loss of *GlcT* appears to have no discernible impact on Notch signaling activity at all. This tissue-
355 specific modulation of Notch signaling by *GlcT* suggests a potential variability in membrane
356 lipid composition across different cell types. Such variability could render certain cells more
357 susceptible to alterations in specific GSLs and their influence on Dl-Notch signaling
358 transduction, while others remain unaffected. As Dl trafficking in *Drosophila* ISCs can be
359 modulated by dietary lipid content, which impacts the duration and level of Notch activation
360 to control the production of EEs in newly enclosed flies [18], the sensitivity of ISCs to specific GSL
361 content may serve as a mechanism enabling ISCs to govern the fate of their progeny based on
362 nutrient content.

363

364 Taken together, our study identified MacCer/LacCer as a tissue-specific regulator of Dl-Notch
365 signaling by regulating the membrane localization and endocytic trafficking of Dl. As Notch
366 signaling has pleiotropic roles in many developmental processes, diseases and cancer, the
367 findings should contribute to our understanding of Notch signaling transduction and may help
368 to open up new approaches for developing prevention and treatments against human diseases
369 and cancer.

370

371
372

373 **ACKNOWLEDGEMENTS**

374 We thank Drs. Feng Yu and Sanduo Zheng for technical assistance, Drs. Dick Nassel, Jan-
375 Adrianus Veenstra, Zhaohui Wang, and the Developmental Studies Hybridoma Bank (DSHB)
376 for antibodies, Drs. Sarah Bray, Steven Hou, Akiko Satoh, Tao Wang, the Bloomington
377 Drosophila Stock Center (BDSC) and Vienna Drosophila Resource Center (VDRC) for fly stocks,
378 and Dr. Sylvie Robine for the villin-Cre^{ERT2} mice. This work was supported by National Key
379 Research and Development Program of China (2020YFA0803502 and 2017YFA0103602 to R.X.)
380 from the Chinese Ministry of Science and Technology.

381

382 **DECLARATION OF INTERESTS**

383 The authors declare no competing interests.

384

385 **MATERIALS AND METHODS**

386 ***Drosophila* Stocks and mice**

387 *Drosophila* melanogaster stocks were maintained on standard cornmeal molasses food in a
388 25°C incubator. Flies for all experiments were maintained at a constant 25°C with 15–25 flies
389 per vial and tossed onto new food every 2–3 days. *Drosophila* stocks used in this study: *hsflp,*
390 *act-GAL4, UAS-GFP; FRT42B tub-GAL80; hsflp, act-GAL4, UAS-GFP; FRT42D tub-GAL80;* and
391 *hsflp, Tub-GAL80, FRT19A; act-GAL4,UAS-GFP/Cyo* [56]; *hsflp; FRT42D, arm-lacZ/Cyo; esg-GAL4,*
392 *UAS-GFP* [56]; *Su(H)GBE (NRE)-GAL4;* and *Dl-Gal4* [57]; *Su(H)GBE-lacZ* (NRE-lacZ, gift from Sarah
393 Bray); *Glc^{EA30}*(generated in this study); *Glc^{E230}*(generated in this study); *GlcT$^{\Delta 8}$* [23]; *Tub-GAL80^{ts}*
394 [58]; *UAS-GlcT* (generated in this study); *GlcT-IR* #1 (VDRC, id:44912); *GlcT-IR* #2 (VDRC,
395 id:108064); *UAS-CDase* (gift from Tao Wang); *UAS-p35* (BDSC, #6298); *egh^{A}* (BDSC, #52353);
396 *egh^{B}* (BDSC, #52354); *egh^{7}* (BDSC, #77889); *brn^{228}* (BDSC, #7392); *β4GalNAcTA-IR* (VDRC,
397 id:4867); *α4GT1-IR* (VDRC, id:2608); *UAS-N^{intra}* [56]; *UAS-GFP-Rab5* (BDSC, #43336); *UAS-Rab7-*
398 *GFP* (BDSC, #42706); *UAS-Rab11-GFP* (BDSC, #8506).

399 Mice used in this study include floxed *UGCG*, which was generated as previously described [47],
400 and villin-CreERT2 [59]. All the research performance underwent strict ethical review and was
401 approved by the Ethics Committee of the National Institute of Biological Sciences, Beijing. Mice
402 were housed at the animal center in the National Institute of Biological Sciences in a Specific

403 Pathogen Free (SPF) facility.

404

405 **EMS Mutagenesis in *Drosophila***

406 EMS mutagenesis was performed as previously described [19, 60]. Briefly, 3~5 day-old, isogenized
407 y w; FRT42B(G13) males were subjected to a 10-hour starvation period before being fed with
408 EMS (ethyl methanesulfonate, 30 mM in sucrose solution applied on filter papers) overnight.
409 Following recovery, these males were mated with *y w; Sco/Cyo* virgin females. In the F1
410 offspring, *y w; FRT42B */Cyo* males were individually mated with several *y w; Sco/Cyo* virgin
411 females. The *y w; FRT42B */Cyo* males and virgin females in the F2 generation were carefully
412 selected and crossed with each other to establish balanced stocks for further genetic studies.
413 Altogether, around 10,000 stocks harboring lethal mutations were obtained and screened.

414

415 **Deficiency Mapping**

416 The complete Bloomington Deficiency Kit for chromosome 2R
417 (https://bdsc.indiana.edu/stocks/df/dfkit-info.html) was used for initial mapping, which
418 helped to localize both the EA30 and E230 lethal mutations to a cytogenetic location between
419 58A3 and 58F1. Subsequent mapping with additional deficiency lines encompassing this
420 region allowed the identification of two small deficiency lines, *Df(2R)Exel7170* and
421 *Df(2R)Excel6078*, which failed to complement both mutations. This refinement narrowed the
422 critical region down to 58B2-58C1. There are 13 protein-coding genes within this region, and
423 genomic sequencing data indicated that both lines carried missense mutations on the *GlcT*
424 gene, as described in the text.

425

426 **Genomic Sequencing and Analysis Method**

427 As all mutants exhibited lethality in the adult stage, homozygous larvae were selected using a
428 green balancer, and the extracted genomic DNAs were sequenced at BGI Genomics using a
429 library with an insert size of ≤800bp. The sequencing platform employed was the HiSeq 2000.
430 For sequence analysis, all mutants were compared to a reference genome. Subsequently,
431 sequencing reads were assigned to each allele based on heterozygote SNPs retained using a
432 custom Perl script. The candidate heterozygous sites were annotated using snpEff.

433

434 **Mosaic Analysis with a Repressible Cell Marker (MARCM) Analysis**

435 To generate MARCM clones [61], flies of the desired genotype were raised and maintained at
436 25°C until they reached 7 days of age. Subsequently, they were subjected to a 60-minute heat
437 shock in a water bath at 37°C. Following the heat shock, the flies were fed with standard food
438 supplemented with yeast paste and this feeding regimen was repeated every 2 days before
439 the flies were dissected for further analysis.

440

441 **GAL4/GAL80^{ts} System**

442 The GAL4/UAS and GAL80ts systems were utilized as previously described [58,62]. To inhibit the
443 GAL4 system, the crosses were sustained at 18°C when employing temperature-sensitive
444 GAL4-mediated RNAi or gene overexpression. Subsequently, F1 adult flies with the correct
445 genotype were transitioned to 29°C to activate the GAL4 system, thereby triggering RNAi or
446 gene overexpression.

447

448 **Tamoxifen Treatment in Mice**

449 Cre recombinase activity was induced via intraperitoneal injection of 2 mg tamoxifen (Sigma-
450 Aldrich, T5648), and tissues were collected 48 hours post-injection. Cre-negative littermates
451 served as controls.

452

453 **Immunofluorescent Staining and Imaging**

454 Adult female midguts were dissected in PBS and fixed for 30 minutes at room temperature in
455 4% paraformaldehyde. The fixed tissues were then dehydrated in methanol for 5 minutes
456 followed by rehydration in a PBT solution (PBS containing 0.1% Triton X-100). The tissues
457 underwent four washes with 0.1% Triton in 1×PBS (PBST) and were subsequently incubated
458 with PBST and primary antibodies overnight at 4°C. After another round of washing, the
459 samples were incubated for 2 hours with secondary antibodies in PBST. Finally, the samples
460 were stained with DAPI for visualization of nuclei.

461 Mouse small intestine was dissected out and gently flushed with cold 1× PBS to remove fecal
462 content, and fixed overnight at 4°C in 4% paraformaldehyde (PFA) prepared in 1× PBS. The

463 tissue was then incubated in a 30% sucrose solution at 4°C for 24 hours, and embedded in OCT
464 (Tissue-Tek) before frozen. Frozen sections of 15 µm thickness were prepared for further
465 analysis. For immunostaining, tissue sections were permeabilized with 1% Triton X-100 (Sigma-
466 Aldrich) in PBS for 1 hour at room temperature (RT), followed by blocking with a solution
467 containing 0.2% Triton X-100, 1% bovine serum albumin (BSA), and 3% goat serum in PBS for
468 1 hour at RT before antibody staining. The sections were mounted in Vectashield mounting
469 media with DAPI (Vector Laboratories) for imaging.

470 Primary antibodies used in this study: mouse anti-Pros (DSHB #MR1A; 1:300); mouse anti-Dl
471 (DSHB Cat#C594.9B; RRID:AB_528194; 1:300); rabbit anti-AstC (gift from Dr. Dick Nassel;
472 1:300); rabbit anti-Tk (gift from Dr. Jan-Adrianus Veenstra; 1:300); Rabbit anti-pH3 (CST Cat#
473 9701; RRID:AB_331535; 1:500); mouse monoclonal anti-β-galactosidase (DSHB, #40-1a; 1:30);
474 mouse anti-Cut (DSHB, #2B10; 1:20); mouse anti-Rab7 (DSHB, 1:300); rabbit anti-pERK (CST,
475 1:200); rabbit anti-STAT92E (gift from Dr. Zhaohui Wang, 1:300); rabbit anti-DCP-1 (CST
476 Cat#9578S; 1:300); mouse monoclonal anti-EYA (DSHB, #10H6; 1:300); rabbit monoclonal anti-
477 GFP (Invitrogen Cat#G10362; 1:300). Secondary antibodies used in this study include Alexa
478 Fluor 568- or Cy5-conjugated goat anti-rabbit, anti-mouse IgGs (Molecular Probes, A11034-
479 A11036, A10524; 1:300). For nuclei staining, DAPI (Sigma-Aldrich, 1 µg/ml) was used. The
480 preparations were mounted in 70% glycerol, and the slides were stored at -20°C. Imaging was
481 conducted using a Leica SP8 confocal microscope. All captured images were processed and
482 compiled using Adobe Photoshop and Illustrator.

483

484 **LacCer Treatment**

485 The 2-3 days old female flies of the specified genotype were moved to fresh food layered with
486 a filter paper soaked in a 5% sucrose solution containing 20 µM of LacCer (Sigma-Aldrich
487 CAS#4682-48-8) and this transfer was repeated daily before dissection and analysis.

488

489 **Antibody Uptake Assay**

490 The anti-Dl antibody Uptake assay was conducted following a previously described protocol [40].
491 In brief, the *Drosophila* gut was dissected and placed in fresh medium containing anti-Delta.
492 The dissecting dish was then placed in a humidified box and incubated at 25 °C for the
493 necessary duration. Subsequently, the medium containing the antibody was removed, and a
494 single wash with Schneider's *Drosophila* medium was carried out. The midgut was then fixed

495 directly in the dissecting dish for 20 minutes under a chemical fume hood by adding 1 ml of
496 fixative. Following this, samples underwent three washes with PBT and were then incubated
497 for 60 minutes with fluorescently labeled anti-mouse secondary antibodies in PBT on a
498 rotating platform. After another three washes with PBT, the samples were mounted in 50%
499 glycerol in PBS for analysis under microscopy.

500

501 **Fluorescence Intensity Statistics**

502 The Image J software (downloaded from https://imagej.nih.gov/ij/) was utilized to measure
503 the fluorescence intensity of the captured images. The corrected fluorescence intensity is
504 determined as the average fluorescence intensity of each cell's nuclear region minus the
505 average background fluorescence intensity.

506

507 **Statistical analysis**

508 All quantifications were presented in the form of mean ± SEM. GraphPad Prism 5 software
509 (GraphPad Software Inc.) was used to calculate p-values using an unpaired Student's t-test.
510 The number of intestines used for calculations was labeled on the figures or in the related
511 figure legends.

512

513 **REFERENCES**

514 1. Bray, S.J. (2006). Notch signalling: a simple pathway becomes complex. Nat Rev Mol Cell Biol *7*,
515 678-689. 10.1038/nrm2009.
516 2. Kopan, R., and Ilagan, M.X. (2009). The canonical Notch signaling pathway: unfolding the
517 activation mechanism. Cell *137*, 216-233. 10.1016/j.cell.2009.03.045.
518 3. Artavanis-Tsakonas, S., Rand, M.D., and Lake, R.J. (1999). Notch signaling: cell fate control and
519 signal integration in development. Science *284*, 770-776.
520 4. Penton, A.L., Leonard, L.D., and Spinner, N.B. (2012). Notch signaling in human development
521 and disease. Semin Cell Dev Biol *23*, 450-457. 10.1016/j.semcdb.2012.01.010.
522 5. Bolos, V., Grego-Bessa, J., and de la Pompa, J.L. (2007). Notch signaling in development and
523 cancer. Endocr Rev *28*, 339-363. 10.1210/er.2006-0046.
524 6. Boumard, B., and Bardin, A.J. (2021). An amuse-bouche of stem cell regulation: Underlying
525 principles and mechanisms from adult Drosophila intestinal stem cells. Curr Opin Cell Biol *73*,
526 58-68. 10.1016/j.ceb.2021.05.007.

527 7. Koch, U., Lehal, R., and Radtke, F. (2013). Stem cells living with a Notch. Development *140*, 689-
528 704. 10.1242/dev.080614.
529 8. Ohlstein, B., and Spradling, A. (2007). Multipotent Drosophila intestinal stem cells specify
530 daughter cell fates by differential notch signaling. Science *315*, 988-992. 315/5814/988
531 [pii10.1126/science.1136606 [doi].
532 9. Ohlstein, B., and Spradling, A. (2006). The adult Drosophila posterior midgut is maintained by
533 pluripotent stem cells. Nature *439*, 470-474. nature04333 [pii]10.1038/nature04333 [doi].
534 10. Chen, J., Xu, N., Wang, C., Huang, P., Huang, H., Jin, Z., Yu, Z., Cai, T., Jiao, R., and Xi, R. (2018).
535 Transient Scute activation via a self-stimulatory loop directs enteroendocrine cell pair
536 specification from self-renewing intestinal stem cells. Nat Cell Biol *20*, 152-161.
537 10.1038/s41556-017-0020-0.
538 11. Micchelli, C.A., and Perrimon, N. (2006). Evidence that stem cells reside in the adult Drosophila
539 midgut epithelium. Nature *439*, 475-479. nature04371 [pii]10.1038/nature04371 [doi].
540 12. Guo, Z., and Ohlstein, B. (2015). Stem cell regulation. Bidirectional Notch signaling regulates
541 Drosophila intestinal stem cell multipotency. Science *350*. 10.1126/science.aab0988.
542 13. Henrique, D., and Schweisguth, F. (2019). Mechanisms of Notch signaling: a simple logic
543 deployed in time and space. Development *146*. 10.1242/dev.172148.
544 14. Yin, C., and Xi, R. (2018). A Phyllopod-Mediated Feedback Loop Promotes Intestinal Stem Cell
545 Enteroendocrine Commitment in Drosophila. Stem Cell Reports *10*, 43-57.
546 10.1016/j.stemcr.2017.11.014.
547 15. Wang, C., Guo, X., Dou, K., Chen, H., and Xi, R. (2015). Ttk69 acts as a master repressor of
548 enteroendocrine cell specification in Drosophila intestinal stem cell lineages. Development *142*,
549 3321-3331. 10.1242/dev.123208.
550 16. Guo, X., Zhang, Y., Huang, H., and Xi, R. (2022). A hierarchical transcription factor cascade
551 regulates enteroendocrine cell diversity and plasticity in Drosophila. Nat Commun *13*, 6525.
552 10.1038/s41467-022-34270-0.
553 17. de Navascues, J., Perdigoto, C.N., Bian, Y., Schneider, M.H., Bardin, A.J., Martinez-Arias, A., and
554 Simons, B.D. (2012). Drosophila midgut homeostasis involves neutral competition between
555 symmetrically dividing intestinal stem cells. EMBO J *31*, 2473-2485. 10.1038/emboj.2012.106.
556 18. Obniski, R., Sieber, M., and Spradling, A.C. (2018). Dietary Lipids Modulate Notch Signaling and
557 Influence Adult Intestinal Development and Metabolism in Drosophila. Dev Cell *47*, 98-111
558 e115. 10.1016/j.devcel.2018.08.013.
559 19. Perdigoto, C.N., Schweisguth, F., and Bardin, A.J. (2011). Distinct levels of Notch activity for
560 commitment and terminal differentiation of stem cells in the adult fly intestine. Development
561 *138*, 4585-4595. dev.065292 [pii]10.1242/dev.065292.
562 20. Ayukawa, T., Matsumoto, K., Ishikawa, H.O., Ishio, A., Yamakawa, T., Aoyama, N., Suzuki, T., and
563 Matsuno, K. (2012). Rescue of Notch signaling in cells incapable of GDP-L-fucose synthesis by
564 gap junction transfer of GDP-L-fucose in Drosophila. Proc Natl Acad Sci U S A *109*, 15318-15323.
565 10.1073/pnas.1202369109.
566 21. Petcherski, A.G., and Kimble, J. (2000). Mastermind is a putative activator for Notch. Curr Biol
567 *10*, R471-473. 10.1016/s0960-9822(00)00577-7.
568 22. Sasamura, T., Ishikawa, H.O., Sasaki, N., Higashi, S., Kanai, M., Nakao, S., Ayukawa, T., Aigaki, T.,
569 Noda, K., Miyoshi, E., et al. (2007). The O-fucosyltransferase O-fut1 is an extracellular

570 component that is essential for the constitutive endocytic trafficking of Notch in Drosophila.
571 Development *134*, 1347-1356. 10.1242/dev.02811.
572 23. Satoh, T., Inagaki, T., Liu, Z., Watanabe, R., and Satoh, A.K. (2013). GPI biosynthesis is essential
573 for rhodopsin sorting at the trans-Golgi network in Drosophila photoreceptors. Development
574 *140*, 385-394. 10.1242/dev.083683.
575 24. Selzner, M., Bielawska, A., Morse, M.A., Rudiger, H.A., Sindram, D., Hannun, Y.A., and Clavien,
576 P.A. (2001). Induction of apoptotic cell death and prevention of tumor growth by ceramide
577 analogues in metastatic human colon cancer. Cancer Res *61*, 1233-1240.
578 25. Ryoo, H.D., Gorenc, T., and Steller, H. (2004). Apoptotic cells can induce compensatory cell
579 proliferation through the JNK and the Wingless signaling pathways. Dev Cell *7*, 491-501.
580 10.1016/j.devcel.2004.08.019.
581 26. Wandall, H.H., Pizette, S., Pedersen, J.W., Eichert, H., Levery, S.B., Mandel, U., Cohen, S.M., and
582 Clausen, H. (2005). Egghead and brainiac are essential for glycosphingolipid biosynthesis in vivo.
583 J Biol Chem *280*, 4858-4863. 10.1074/jbc.C400571200.
584 27. Muller, R., Altmann, F., Zhou, D., and Hennet, T. (2002). The Drosophila melanogaster brainiac
585 protein is a glycolipid-specific beta 1,3N-acetylglucosaminyltransferase. J Biol Chem *277*,
586 32417-32420. 10.1074/jbc.C200381200.
587 28. Stolz, A., Haines, N., Pich, A., Irvine, K.D., Hokke, C.H., Deelder, A.M., Gerardy-Schahn, R.,
588 Wuhrer, M., and Bakker, H. (2008). Distinct contributions of beta 4GalNAcTA and beta
589 4GalNAcTB to Drosophila glycosphingolipid biosynthesis. Glycoconj J *25*, 167-175.
590 10.1007/s10719-007-9069-5.
591 29. Chen, Y.W., Pedersen, J.W., Wandall, H.H., Levery, S.B., Pizette, S., Clausen, H., and Cohen, S.M.
592 (2007). Glycosphingolipids with extended sugar chain have specialized functions in
593 development and behavior of Drosophila. Dev Biol *306*, 736-749. 10.1016/j.ydbio.2007.04.013.
594 30. Xu, N., Wang, S.Q., Tan, D., Gao, Y., Lin, G., and Xi, R. (2011). EGFR, Wingless and JAK/STAT
595 signaling cooperatively maintain Drosophila intestinal stem cells. Dev Biol *354*, 31-43. S0012-
596 1606(11)00182-5 [pii]10.1016/j.ydbio.2011.03.018 [doi].
597 31. Jiang, H., Patel, P.H., Kohlmaier, A., Grenley, M.O., McEwen, D.G., and Edgar, B.A. (2009).
598 Cytokine/Jak/Stat signaling mediates regeneration and homeostasis in the Drosophila midgut.
599 Cell *137*, 1343-1355. S0092-8674(09)00571-6 [pii]10.1016/j.cell.2009.05.014 [doi].
600 32. Ohlstein, B., and Spradling, A. (2007). Multipotent Drosophila intestinal stem cells specify
601 daughter cell fates by differential notch signaling. Science *315*, 988-992.
602 33. Guo, Z., and Ohlstein, B. (2015). Bidirectional Notch signaling regulates Drosophila intestinal
603 stem cell multipotency. Science *350*, aab0988.
604 34. Jiang, H., Grenley, M.O., Bravo, M.J., Blumhagen, R.Z., and Edgar, B.A. (2011). EGFR/Ras/MAPK
605 signaling mediates adult midgut epithelial homeostasis and regeneration in Drosophila. Cell
606 Stem Cell *8*, 84-95.
607 35. Patel, P.H., Dutta, D., and Edgar, B.A. (2015). Niche appropriation by Drosophila intestinal stem
608 cell tumours. Nat Cell Biol *17*, 1182-1192. 10.1038/ncb3214.
609 36. Beehler-Evans, R., and Micchelli, C.A. (2015). Generation of enteroendocrine cell diversity in
610 midgut stem cell lineages. Development *142*, 654-664. 10.1242/dev.114959.
611 37. Bray, S.J., and Gomez-Lamarca, M. (2018). Notch after cleavage. Current opinion in cell biology
612 *51*, 103-109.

613 38. Yamamoto, S., Charng, W.L., and Bellen, H.J. (2010). Endocytosis and intracellular trafficking of
614 Notch and its ligands. Curr Top Dev Biol *92*, 165-200. 10.1016/S0070-2153(10)92005-X.
615 39. Simons, K., and Toomre, D. (2000). Lipid rafts and signal transduction. Nat Rev Mol Cell Biol *1*,
616 31-39. 10.1038/35036052.
617 40. Couturier, L., and Schweisguth, F. (2014). Antibody uptake assay and in vivo imaging to study
618 intracellular trafficking of Notch and Delta in Drosophila. Methods Mol Biol *1187*, 79-86.
619 10.1007/978-1-4939-1139-4_6.
620 41. Micchelli, C.A., Rulifson, E.J., and Blair, S.S. (1997). The function and regulation of cut
621 expression on the wing margin of Drosophila: Notch, Wingless and a dominant negative role
622 for Delta and Serrate. Development *124*, 1485-1495.
623 42. Deng, W.-M., Althauser, C., and Ruohola-Baker, H. (2001). Notch-Delta signaling induces a
624 transition from mitotic cell cycle to endocycle in Drosophila follicle cells.
625 43. López-Schier, H., and Johnston, D.S. (2001). Delta signaling from the germ line controls the
626 proliferation and differentiation of the somatic follicle cells during Drosophila oogenesis. Genes
627 & development *15*, 1393-1405.
628 44. van Es, J.H., van Gijn, M.E., Riccio, O., van den Born, M., Vooijs, M., Begthel, H., Cozijnsen, M.,
629 Robine, S., Winton, D.J., Radtke, F., and Clevers, H. (2005). Notch/gamma-secretase inhibition
630 turns proliferative cells in intestinal crypts and adenomas into goblet cells. Nature *435*, 959-
631 963.
632 45. Riccio, O., van Gijn, M.E., Bezdek, A.C., Pellegrinet, L., van Es, J.H., Zimber-Strobl, U., Strobl, L.J.,
633 Honjo, T., Clevers, H., and Radtke, F. (2008). Loss of intestinal crypt progenitor cells owing to
634 inactivation of both Notch1 and Notch2 is accompanied by derepression of CDK inhibitors
635 p27Kip1 and p57Kip2. EMBO Rep *9*, 377-383. 10.1038/embor.2008.7.
636 46. Fre, S., Huyghe, M., Mourikis, P., Robine, S., Louvard, D., and Artavanis-Tsakonas, S. (2005).
637 Notch signals control the fate of immature progenitor cells in the intestine. Nature *435*, 964-
638 968.
639 47. Jennemann, R., Kaden, S., Sandhoff, R., Nordstrom, V., Wang, S., Volz, M., Robine, S., Amen, N.,
640 Rothermel, U., Wiegandt, H., and Grone, H.J. (2012). Glycosphingolipids are essential for
641 intestinal endocytic function. J Biol Chem *287*, 32598-32616. 10.1074/jbc.M112.371005.
642 48. VanDussen, K.L., Carulli, A.J., Keeley, T.M., Patel, S.R., Puthoff, B.J., Magness, S.T., Tran, I.T.,
643 Maillard, I., Siebel, C., Kolterud, A., et al. (2012). Notch signaling modulates proliferation and
644 differentiation of intestinal crypt base columnar stem cells. Development *139*, 488-497.
645 10.1242/dev.070763.
646 49. Coskun, U., Grzybek, M., Drechsel, D., and Simons, K. (2011). Regulation of human EGF receptor
647 by lipids. Proc Natl Acad Sci U S A *108*, 9044-9048. 10.1073/pnas.1105666108.
648 50. Hamel, S., Fantini, J., and Schweisguth, F. (2010). Notch ligand activity is modulated by
649 glycosphingolipid membrane composition in Drosophila melanogaster. J Cell Biol *188*, 581-594.
650 10.1083/jcb.200907116.
651 51. Ideo, H., Seko, A., Ishizuka, I., and Yamashita, K. (2003). The N-terminal carbohydrate
652 recognition domain of galectin-8 recognizes specific glycosphingolipids with high affinity.
653 Glycobiology *13*, 713-723. 10.1093/glycob/cwg094.
654 52. Park, S.Y., Kwak, C.Y., Shayman, J.A., and Kim, J.H. (2012). Globoside promotes activation of ERK
655 by interaction with the epidermal growth factor receptor. Biochim Biophys Acta *1820*, 1141-
656 1148. 10.1016/j.bbagen.2012.04.008.

657 53. Suckling, R.J., Korona, B., Whiteman, P., Chillakuri, C., Holt, L., Handford, P.A., and Lea, S.M.
658 (2017). Structural and functional dissection of the interplay between lipid and Notch binding
659 by human Notch ligands. EMBO J *36*, 2204-2215. 10.15252/embj.201796632.
660 54. Martins, T., Meng, Y., Korona, B., Suckling, R., Johnson, S., Handford, P.A., Lea, S.M., and Bray,
661 S.J. (2021). The conserved C2 phospholipid-binding domain in Delta contributes to robust
662 Notch signalling. EMBO Rep *22*, e52729. 10.15252/embr.202152729.
663 55. Chillakuri, C.R., Sheppard, D., Ilagan, M.X., Holt, L.R., Abbott, F., Liang, S., Kopan, R., Handford,
664 P.A., and Lea, S.M. (2013). Structural analysis uncovers lipid-binding properties of Notch ligands.
665 Cell Rep *5*, 861-867. 10.1016/j.celrep.2013.10.029.
666 56. Lin, G., Xu, N., and Xi, R. (2008). Paracrine Wingless signalling controls self-renewal of
667 Drosophila intestinal stem cells. Nature *455*, 1119-1123. nature07329
668 [pii]10.1038/nature07329 [doi].
669 57. Zeng, X., Chauhan, C., and Hou, S.X. (2010). Characterization of midgut stem cell- and
670 enteroblast-specific Gal4 lines in drosophila. Genesis *48*, 607-611. 10.1002/dvg.20661 [doi].
671 58. McGuire, S.E., Mao, Z., and Davis, R.L. (2004). Spatiotemporal gene expression targeting with
672 the TARGET and gene-switch systems in Drosophila. Sci STKE *2004*, pl6.
673 59. el Marjou, F., Janssen, K.P., Chang, B.H., Li, M., Hindie, V., Chan, L., Louvard, D., Chambon, P.,
674 Metzger, D., and Robine, S. (2004). Tissue-specific and inducible Cre-mediated recombination
675 in the gut epithelium. Genesis *39*, 186-193. 10.1002/gene.20042.
676 60. Gervais, L. et al. Stem Cell Proliferation Is Kept in Check by the Chromatin Regulators
677 Kismet/CHD7/CHD8 and Trr/MLL3/4. Dev Cell 49, 556-573 e556,
678 doi:10.1016/j.devcel.2019.04.033 (2019).
679 61. Lee, T., and Luo, L. (1999). Mosaic analysis with a repressible cell marker for studies of gene
680 function in neuronal morphogenesis. Neuron *22*, 451-461. S0896-6273(00)80701-1 [pii].
681 62. Brand, A.H., and Perrimon, N. (1993). Targeted gene expression as a means of altering cell fates
682 and generating dominant phenotypes. Development *118*, 401-415.

683

684 **Figure legends**

685 **Figure 1. A mosaic genetic screen identifies *GlcT* as a tumor suppressor in adult *Drosophila***
686 **midgut**

687 (**A**) Diagram showing the lineage hierarchy of intestinal stem cells (ISCs) in the Drosophila
688 intestine. Abbreviations: EB, enteroblast; EEP, enteroendocrine progenitor; EC, enterocyte; EE,
689 enteroendocrine cell. (**B** to **D**) MARCM clones (green) induced for 5 days with Pros (red)
690 staining (B), together with quantification of cell number (C) and the percentage of $Pros^+$ EE
691 cells per clone (D) in *EA30*, *E230*, and *GlcT* null allele ($GlcT^{\Delta 8}$) mutant. (**E** to **F**) Overexpression
692 of *GlcT* in *EA30* or *E230* mutant clones with Pros staining, along with quantification of the
693 percentage of $Pros^+$ EE cells per clone (F). (**G** to **J**) *esg>GlcT-IR* in adult fly gut for 14 days. PH3
694 staining (G) and Pros staining (I) with quantification of positively stained cells. Error bars
695 represent mean ± SEM, with p-values indicated in the figure (two-tailed Student's t-test). Scale
696 bars: 25 µm.

697

698 **Figure 2. Genetic analysis of the components of the GSL synthesis pathway reveals specific**
699 **tumor-suppressive activity for *egh*, in addition to *GlcT***

700 (**A**) Diagram illustrating a portion of the glycosphingolipid (GSL) metabolic pathway
701 synthesized from ceramide, highlighting the key enzymes involved at each step. (**B** to **D**) $GlcT^{\Delta 8}$
702 clones induced for 7 days without or with co-expression of p35 or CDase, stained with anti-
703 DCP-1 or anti-Pros (B). Quantification of the percentage of $Pros^+$ cells in clones of the indicated
704 genotypes (C, D). (**E** to **G**) MARCM clones induced in several mutants of key enzymes in the
705 GSL synthesis pathway. Pros staining in *egh* mutant clones (egh^A, egh^B, egh^7), brn^{228},
706 *β4GalNAcTA-IR*, and *α4GT1-IR* clones (E). Quantification of cell number (F) and the percentage
707 of $Pros^+$ cells (G) in clones of the indicated genotypes. Error bars represent mean ± SEM, with
708 p-values indicated (two-tailed Student's t-test). Scale bars: 25 µm.

709

710 **Figure 3. The EE tumor phenotype is a result of MacCer deficiency**

711 (**A** to **C**) LacCer feeding after MARCM clone induction. Anti-Pros staining of anterior midgut
712 (AM) and posterior midgut (PM) in *GlcT*$^{\Delta 8}$ clones (A). Quantification of cell number (B) and the
713 percentage of Pros^{+} cells (C) in clones of the indicated genotypes. Error bars represent mean
714 ± SEM, with p-values indicated (two-tailed Student's t-test). Scale bars: 25 µm.

715

716 **Figure 4. Loss of *GlcT* leads to reduced activation of Notch signaling in ISC progenies**

717 (**A** and **B**) Expression of NRE-lacZ, the Notch activity reporter, in *GlcT*$^{\Delta 8}$ clones (A) and
718 quantification of LacZ fluorescence intensity for signal positive cell (B). (**C**) Tk and AstC staining
719 in *GlcT*$^{\Delta 8}$ clones in the posterior (R5) region of the Drosophila midgut. (**D**) Pros staining in *N*^{intra}-
720 overexpressing *GlcT*$^{\Delta 8}$ clones. Error bars represent mean ± SEM, with p-values indicated (two-
721 tailed Student's t-test). Scale bars: 25 µm.

722

723 **Figure 5. *GlcT* regulates the endocytic trafficking of Delta**

724 (**A** and **B**) Pros staining in flies carrying *GlcT-IR* driven by *Dl*^{ts} and *NRE*^{ts} respectively (A), and
725 quantification of the percentage of Pros^{+} cells (B). (**C** and **D**) Dl staining in an antibody uptake
726 assay performed in *GlcT*$^{\Delta 8}$ flies after 3-hour clone induction (C) and quantification of Dl
727 fluorescence intensity inside and outside of the clones (D). (**E** and **F**) Dl staining in *esg>GlcT-IR*
728 flies co-stained with Rab5-GFP, Rab7-GFP or Rab11-GFP (E); yellow arrows indicate co-
729 localization of Dl and GFP. Quantification of Dl and GFP co-localization (F). Error bars represent
730 mean ± SEM, with p-values indicated (two-tailed Student's t-test). Scale bars: 25 µm (10 µm in
731 E).

732

733 **Figure 6. *GlcT* shows tissue specificity in regulating Notch signaling activity**

734 (**A**) Cut staining in wing disc of *GlcT*$^{\Delta 8}$ clones. (**B**) EYA staining in follicle cell clones (non-green
735 areas) of *GlcT*$^{\Delta 8}$ flies. (**C**) Dl staining in germ cell clones (non-green area) of *GlcT*$^{\Delta 8}$ mutant clone ,
736 yellow arrows indicate punctate Dl accumulation. Scale bars: 25 µm.

737

738 **Figure 7. Transient loss of *UGCG* in mouse small intestine causes reduced number of ISCs and**
739 **increased number of goblet cells**

740 (**A** and **B**) Olfm4 staining in the duodenum and ileum of *Villin*^{CreERT2}*; UGCG*$^{flox/flox}$ mice 48 hours
741 after tamoxifen injection (n = 3, A) and quantification of Olfm4 fluorescence intensity (B). (**C**
742 and **D**) Muc2 staining of goblet cells in the duodenum and ileum of *UGCG-CKO* mice (C) and
743 quantification of Muc2^{+} goblet cells per villus (D). (**E**) Schematic model illustrating the role of
744 MacCer in regulating the Notch signaling pathway. Error bars represent mean ± SEM, with p-
745 values indicated (two-tailed Student's t-test). Scale bars: 100 µm.

746 **Figure 1—Supplementary Figure 1. Cross scheme for the mosaic genetic screen on the 2R**
747 **chromosome.**

748 (A) A schematic illustrating the principles of FLPase-induced mitotic recombination for
749 generating homozygous mutant cells in heterozygous animals. (B) The cross scheme and
750 workflow for the forward genetic mosaic screen conducted in this study. Abbreviation: EMS,
751 ethyl methanesulfonate.

752

753 **Figure 4—Supplementary Figure 2. The EGFR/Ras/MAPK and JAK/STAT signaling activities in**
754 ***GlcT* mutant clones.**

755 *GlcT* mutant clones stained with pERK (red, upper panels), a direct indicator of
756 EGFR/Ras/MAPK signaling activity, and STAT92E (red, lower panels), whose nuclear localization
757 is indicative of JAK/STAT signaling activity. Note that pERK was not significantly increased in
758 *GlcT* mutant cells compared to normal cells outside of the clones, and STAT92E activity was
759 also not obviously altered in *GlcT* mutant cells compared to normal cells outside the clones.
760 Scale bar: 25 µm.

761

762 **Figure 7— Supplementary Figure 3. The Crypt-Villus morphology in *UGCG* CKO mice. The**
763 **duodenal structure exhibits significant abnormalities in *CKO* mice**

764 Small intestine (duodenum) from control and *villin-creERT2, UGCG*$^{flox/flox}$ mice stained with K20,
765 which marks enterocytes and goblet cells, and Ki67, which marks proliferative cells. Note that
766 the mutant intestine has shortened villi and elongated crypts. Dotted lines indicate the
767 boundary between the crypt and the villus. Samples were collected at 48h after tamoxifen
768 injection. Scale bar: 100 µm.

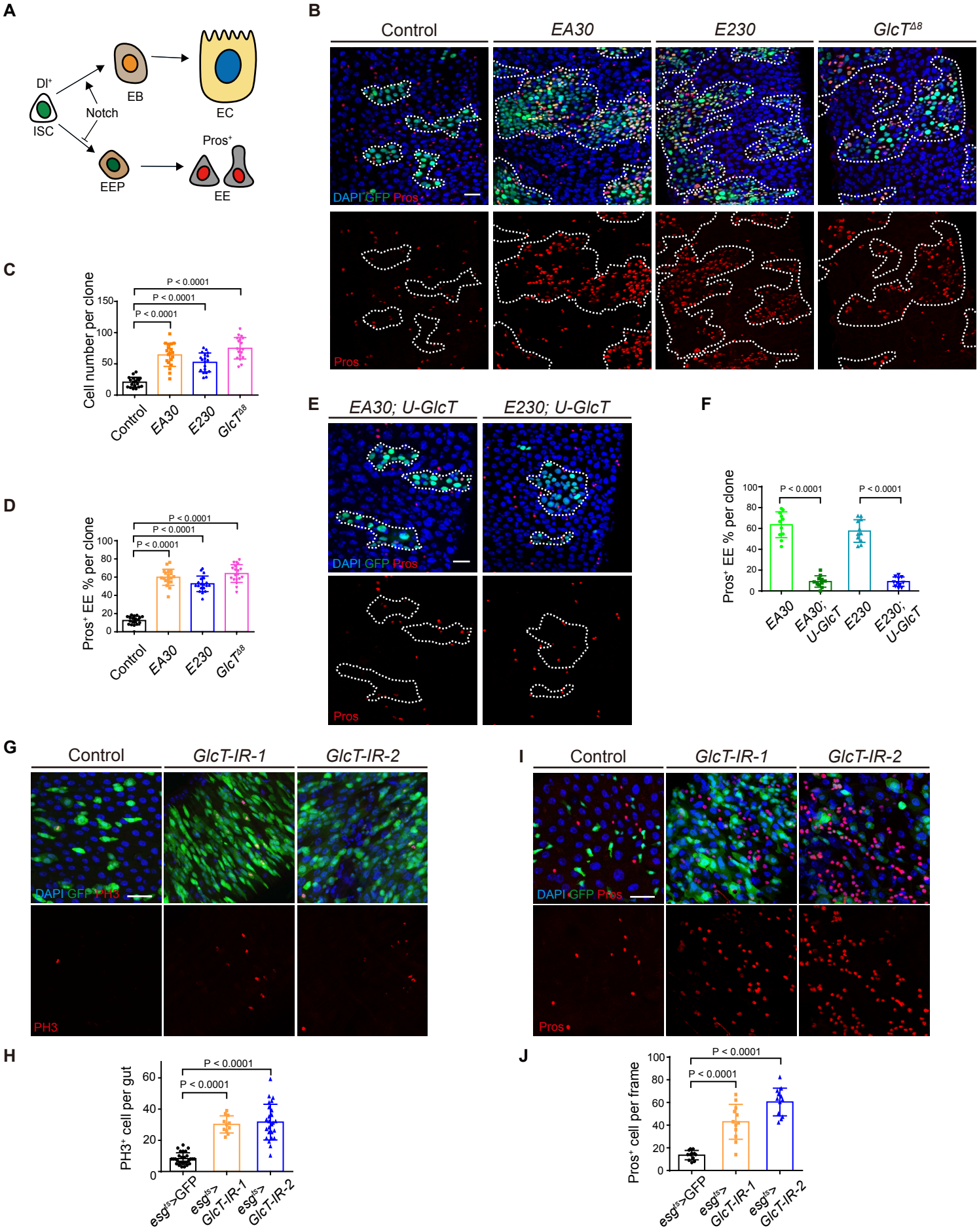
A
Dl+
ISC
Notch
EB
EC
EEP
Pros+
EE
B
Control
EA30
E230
GlcTΔ8
DAPI GFP Pros
Pros
C
Cell number per clone
P < 0.0001
P < 0.0001
P < 0.0001
Control
EA30
E230
GlcTΔ8
D
Pros+ EE % per clone
P < 0.0001
P < 0.0001
P < 0.0001
Control
EA30
E230
GlcTΔ8
E
EA30; U-GlcT
E230; U-GlcT
DAPI GFP Pros
Pros
F
Pros+ EE % per clone
P < 0.0001
P < 0.0001
EA30
EA30; U-GlcT
E230
E230; U-GlcT
G
Control
GlcT-IR-1
GlcT-IR-2
DAPI GFP PH3
PH3
H
PH3+ cell per gut
P < 0.0001
P < 0.0001
esgts>GFP
esgts> GlcT-IR-1
esgts> GlcT-IR-2
I
Control
GlcT-IR-1
GlcT-IR-2
DAPI GFP Pros
Pros
J
Pros+ cell per frame
P < 0.0001
P < 0.0001
esgts>GFP
esgts> GlcT-IR-1
esgts> GlcT-IR-2

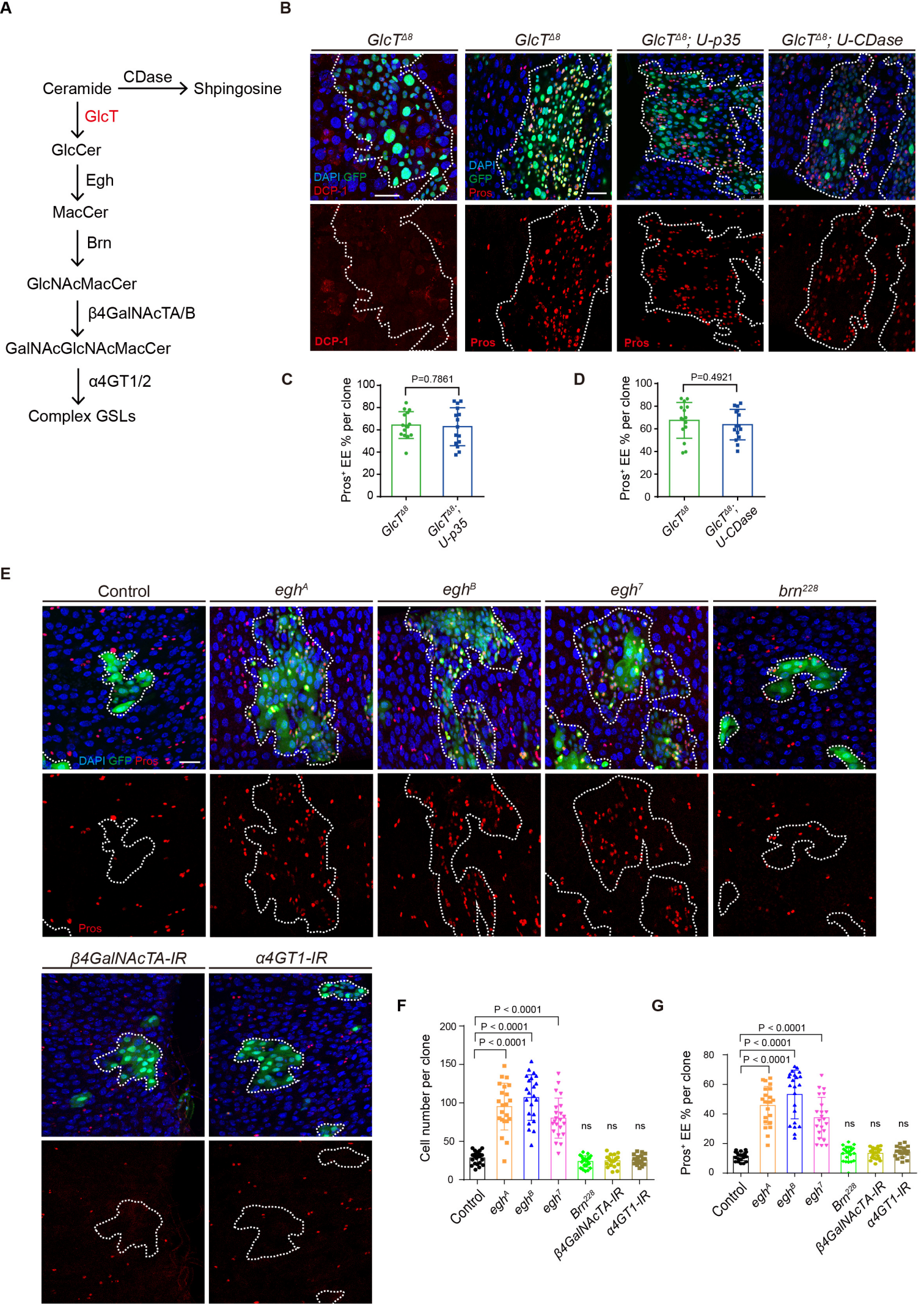
A
Ceramide
CDase
Shpingosine
GlcT
GlcCer
Egh
MacCer
Brn
GlcNAcMacCer
β4GalNAcTA/B
GalNAcGlcNAcMacCer
α4GT1/2
Complex GSLs
B
GlcT$^{\Delta 8}$
GlcT$^{\Delta 8}$
GlcT$^{\Delta 8}$; U-p35
GlcT$^{\Delta 8}$; U-CDase
DAPI GFP
DCP-1
DAPI
GFP
Pros
DCP-1
Pros
Pros
C
P=0.7861
Pros$^+$ EE % per clone
GlcT$^{\Delta 8}$
GlcT$^{\Delta 8}$; U-p35
D
P=0.4921
Pros$^+$ EE % per clone
GlcT$^{\Delta 8}$
GlcT$^{\Delta 8}$; U-CDase
E
Control
egh^A
egh^B
egh^7
brn^{228}
DAPI GFP Pros
Pros
β4GalNAcTA-IR
α4GT1-IR
F
Cell number per clone
P < 0.0001
P < 0.0001
P < 0.0001
ns
ns
ns
Control
egh^A
egh^B
egh^7
Brn^{228}
β4GalNAcTA-IR
α4GT1-IR
G
Pros$^+$ EE % per clone
P < 0.0001
P < 0.0001
P < 0.0001
ns
ns
ns
Control
egh^A
egh^B
egh^7
Brn^{228}
β4GalNAcTA-IR
α4GT1-IR

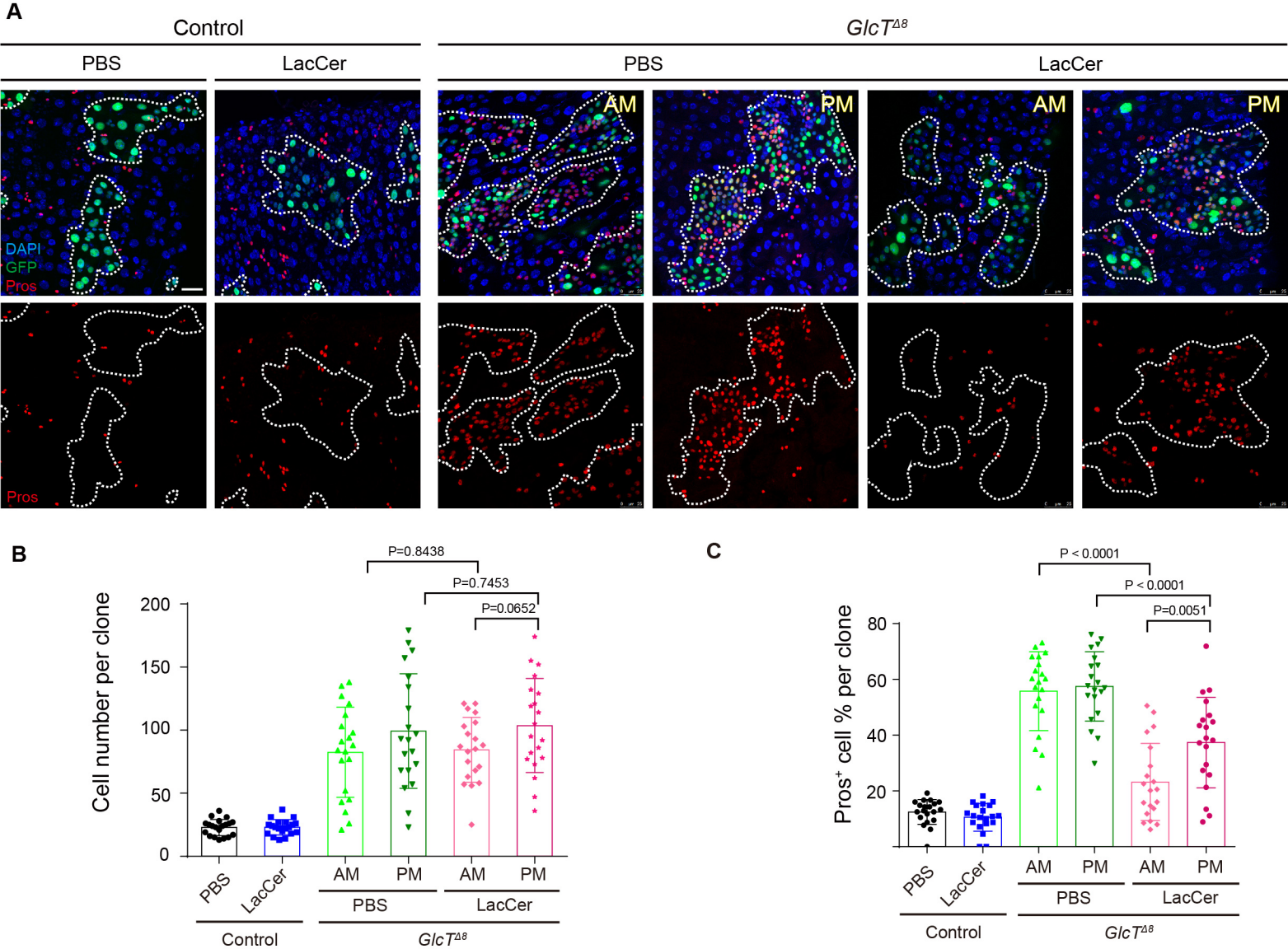
A
Control
GlcT^Δ8
PBS
LacCer
PBS
LacCer
AM
PM
AM
PM
DAPI
GFP
Pros
Pros
B
P=0.8438
P=0.7453
P=0.0652
Cell number per clone
200
150
100
50
0
PBS
LacCer
AM
PM
AM
PM
PBS
LacCer
Control
GlcT^Δ8
C
P < 0.0001
P < 0.0001
P=0.0051
Pros+ cell % per clone
80
60
40
20
PBS
LacCer
AM
PM
AM
PM
PBS
LacCer
Control
GlcT^Δ8

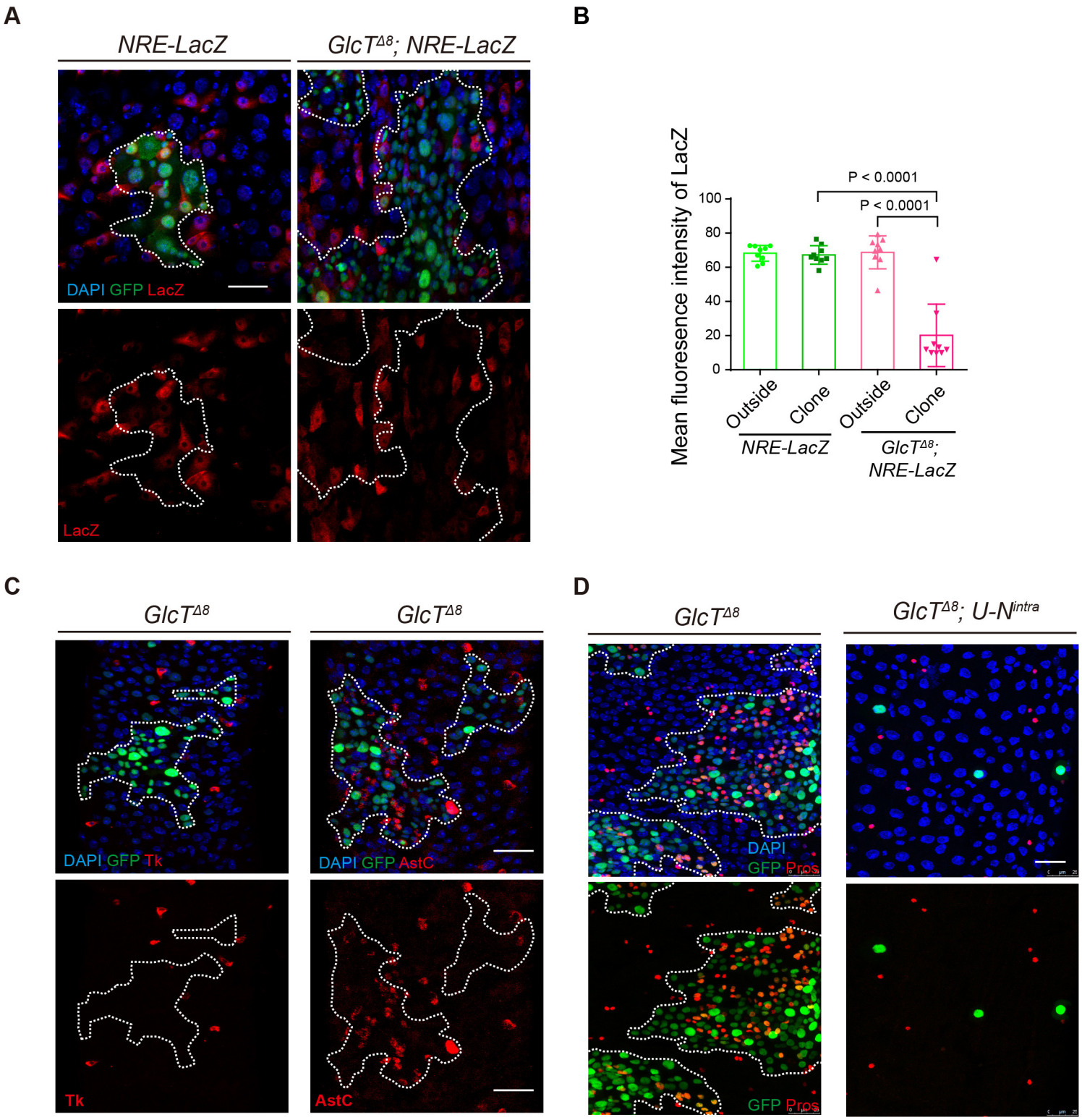
A
NRE-LacZ
GlcT$^{\Delta 8}$; NRE-LacZ
DAPI GFP LacZ
LacZ
B
Mean fluorescence intensity of LacZ
P < 0.0001
P < 0.0001
100
80
60
40
20
0
Outside
Clone
Outside
Clone
NRE-LacZ
GlcT$^{\Delta 8}$; NRE-LacZ
C
GlcT$^{\Delta 8}$
GlcT$^{\Delta 8}$
DAPI GFP Tk
DAPI GFP AstC
Tk
AstC
D
GlcT$^{\Delta 8}$
GlcT$^{\Delta 8}$; U-N^{intra}
DAPI
GFP Pros
GFP Pros

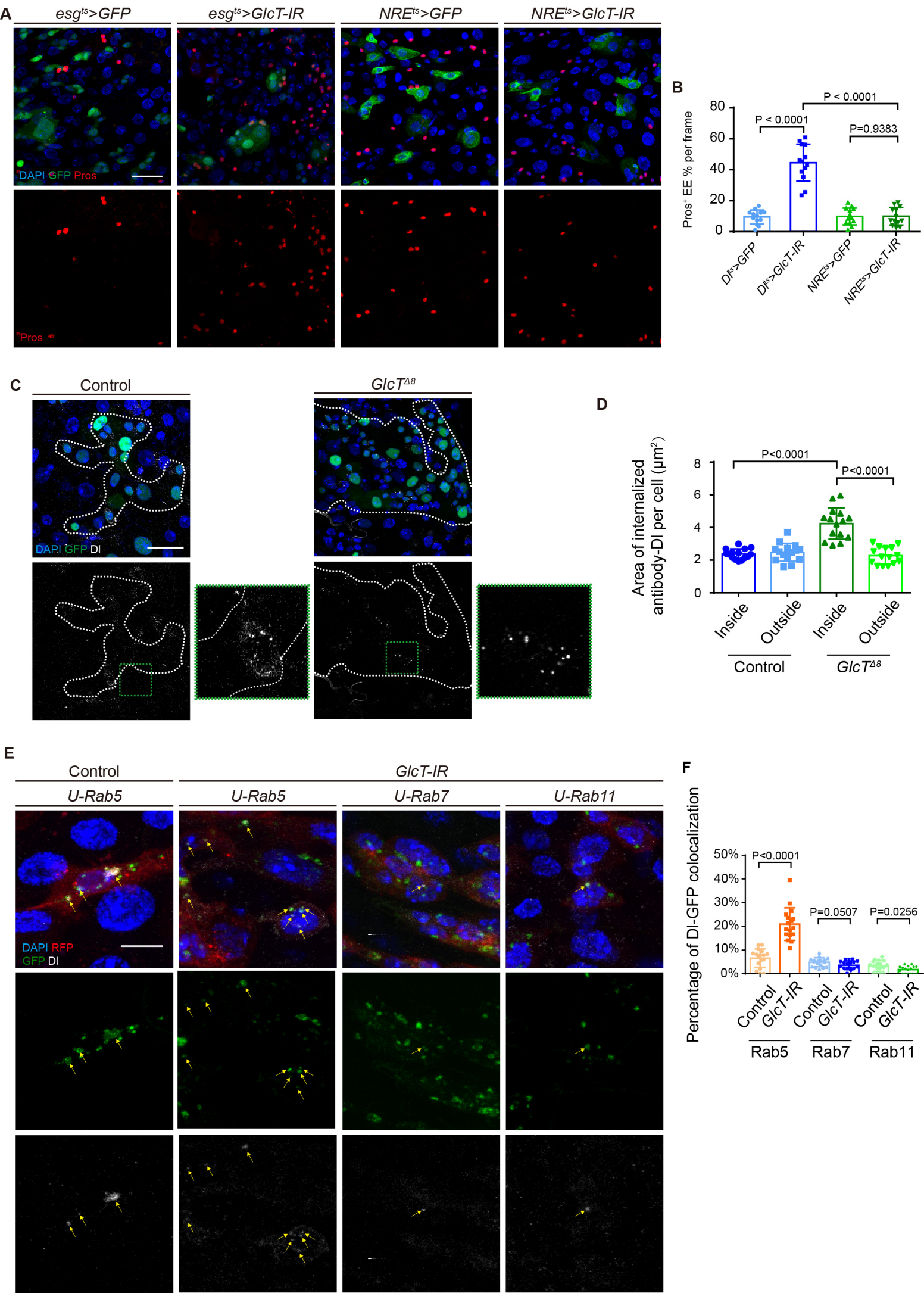
A
esg^ts>GFP
esg^ts>GlcT-IR
NRE^ts>GFP
NRE^ts>GlcT-IR
DAPI GFP Pros
Pros
B
Pros+ EE % per frame
P < 0.0001
P < 0.0001
P=0.9383
Dl^ts>GFP
Dl^ts>GlcT-IR
NRE^ts>GFP
NRE^ts>GlcT-IR
C
Control
GlcT^Δ8
DAPI GFP Dl
D
Area of internalized antibody-Dl per cell (μm²)
P<0.0001
P<0.0001
Inside
Outside
Inside
Outside
Control
GlcT^Δ8
E
Control
GlcT-IR
U-Rab5
U-Rab5
U-Rab7
U-Rab11
DAPI RFP
GFP Dl
F
Percentage of Dl-GFP colocalization
P<0.0001
P=0.0507
P=0.0256
Control
GlcT-IR
Control
GlcT-IR
Control
GlcT-IR
Rab5
Rab7
Rab11

A

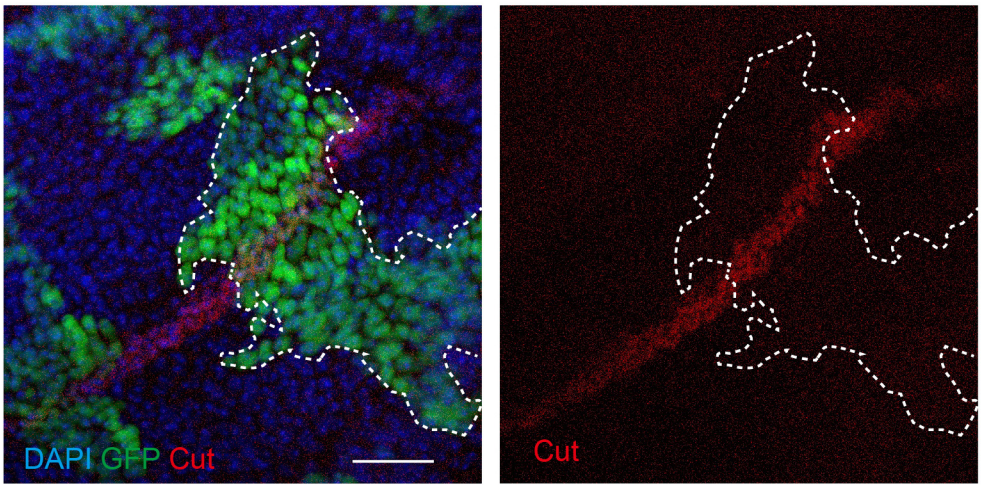

B

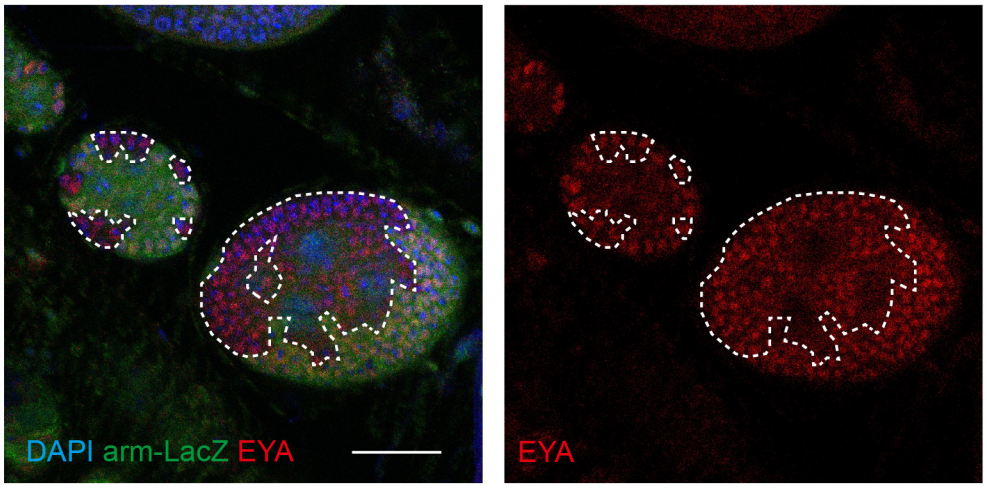

C

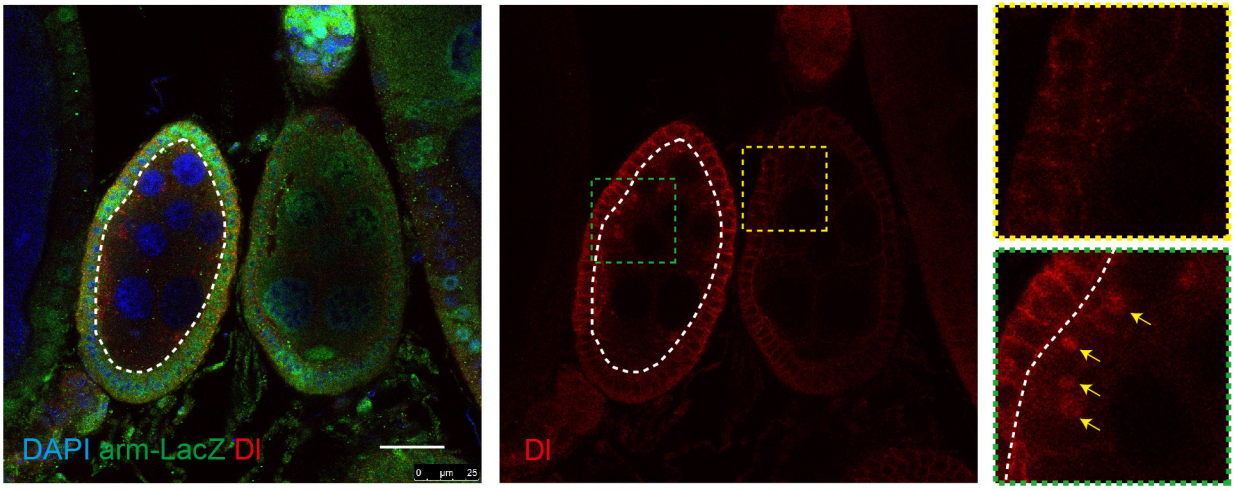

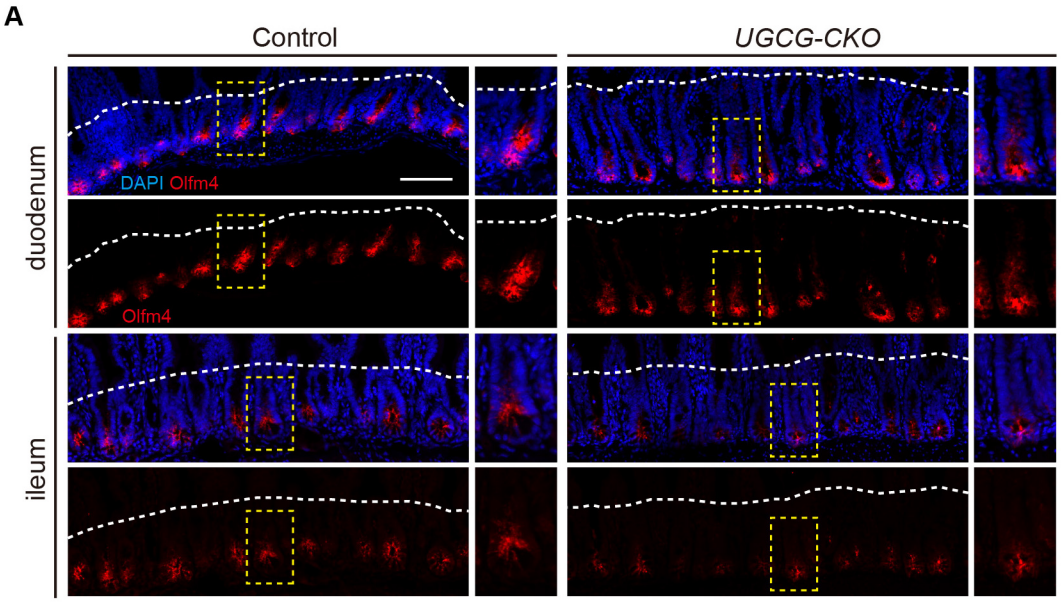
A
Control
UGCG-CKO
duodenum
ileum
DAPI Olfm4
Olfm4

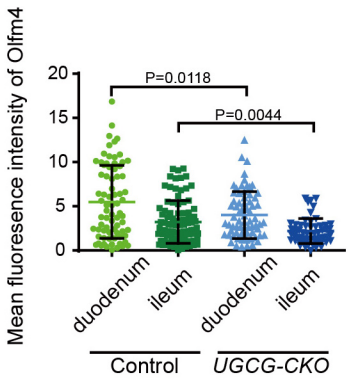
B
Mean fluoresence intensity of Olfm4
20
15
10
5
0
P=0.0118
P=0.0044
duodenum
ileum
duodenum
ileum
Control
UGCG-CKO

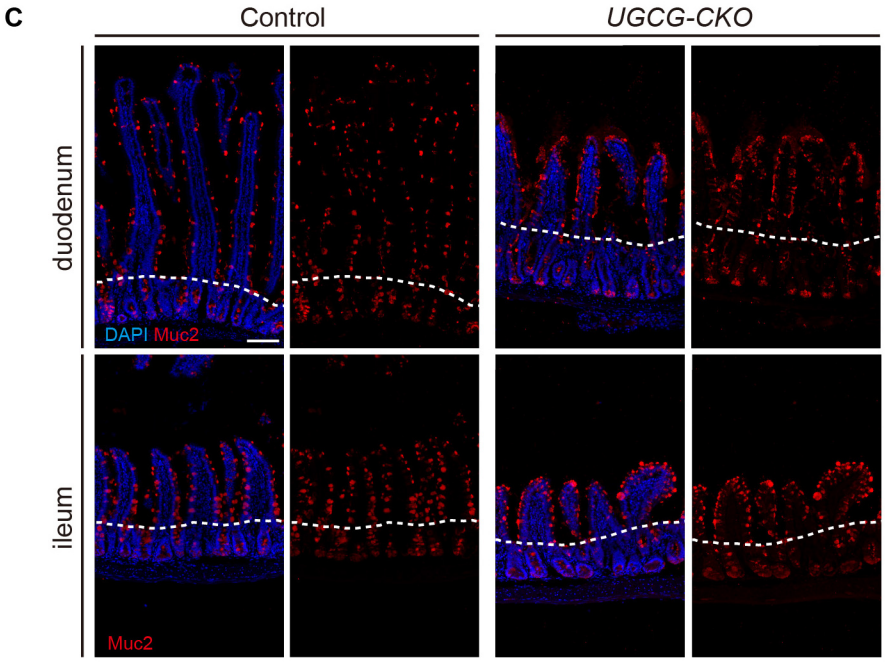
C
Control
UGCG-CKO
duodenum
ileum
DAPI Muc2
Muc2

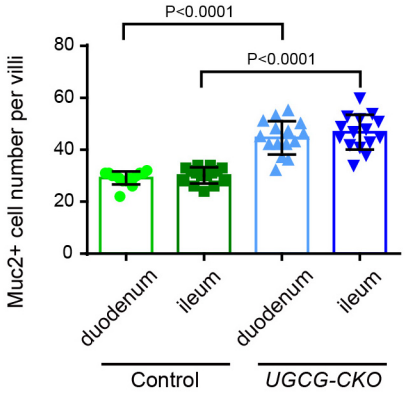
D
Muc2+ cell number per villi
80
60
40
20
0
P<0.0001
P<0.0001
duodenum
ileum
duodenum
ileum
Control
UGCG-CKO

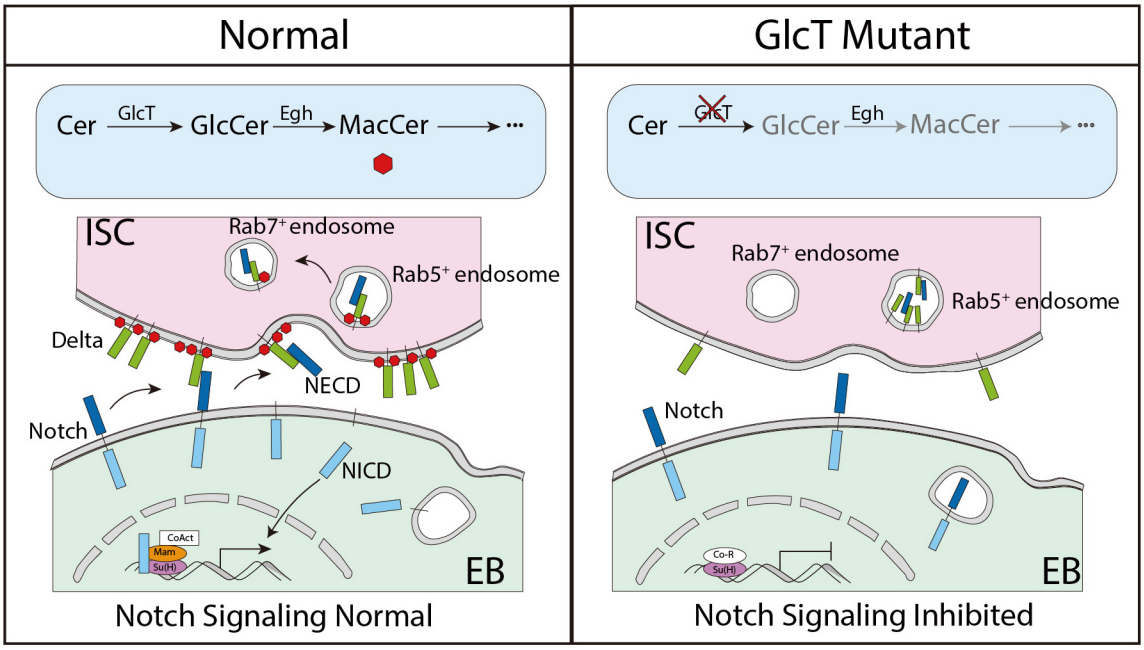
E
Normal
GlcT Mutant
Cer
GlcT
GlcCer
Egh
MacCer
ISC
Rab7⁺ endosome
Rab5⁺ endosome
Delta
NECD
Notch
NICD
CoAct
Mam
Su(H)
EB
Notch Signaling Normal
Co-R
Notch Signaling Inhibited

A

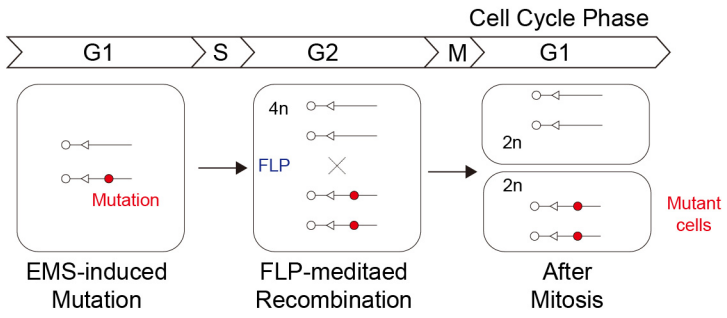
Cell Cycle Phase
G1
S
G2
M
G1
Mutation
4n
FLP
2n
2n
Mutant cells
EMS-induced Mutation
FLP-meditaed Recombination
After Mitosis

B

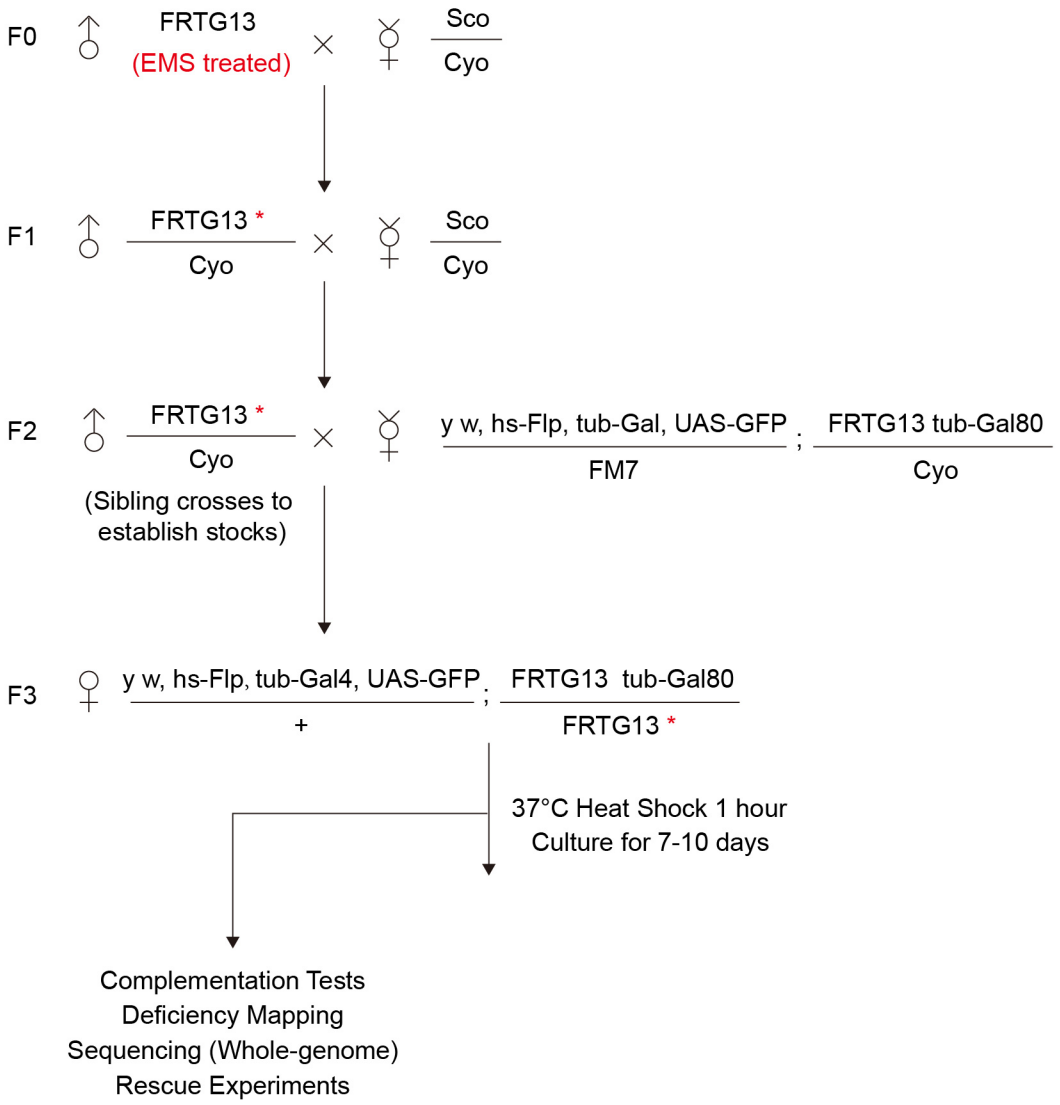
F0
FRTG13
(EMS treated)
Sco
Cyo
F1
FRTG13 *
Cyo
Sco
Cyo
F2
FRTG13 *
Cyo
(Sibling crosses to establish stocks)
y w, hs-Flp, tub-Gal, UAS-GFP
FM7
FRTG13 tub-Gal80
Cyo
F3
y w, hs-Flp, tub-Gal4, UAS-GFP
+
FRTG13 tub-Gal80
FRTG13 *
37°C Heat Shock 1 hour
Culture for 7-10 days
Complementation Tests
Deficiency Mapping
Sequencing (Whole-genome)
Rescue Experiments

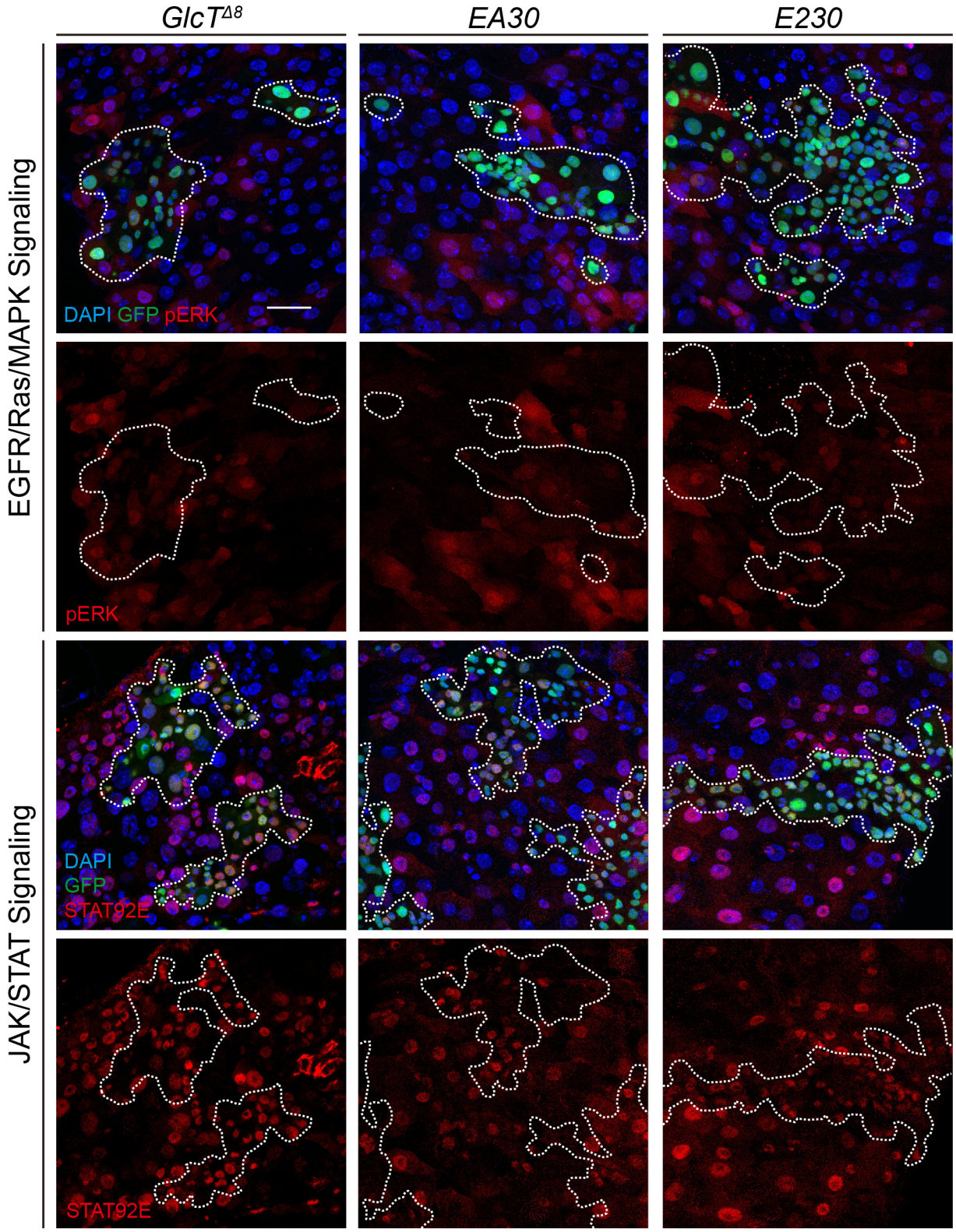
GlcT$^{\Delta 8}$
EA30
E230
EGFR/Ras/MAPK Signaling
DAPI GFP pERK
pERK
JAK/STAT Signaling
DAPI
GFP
STAT92E
STAT92E

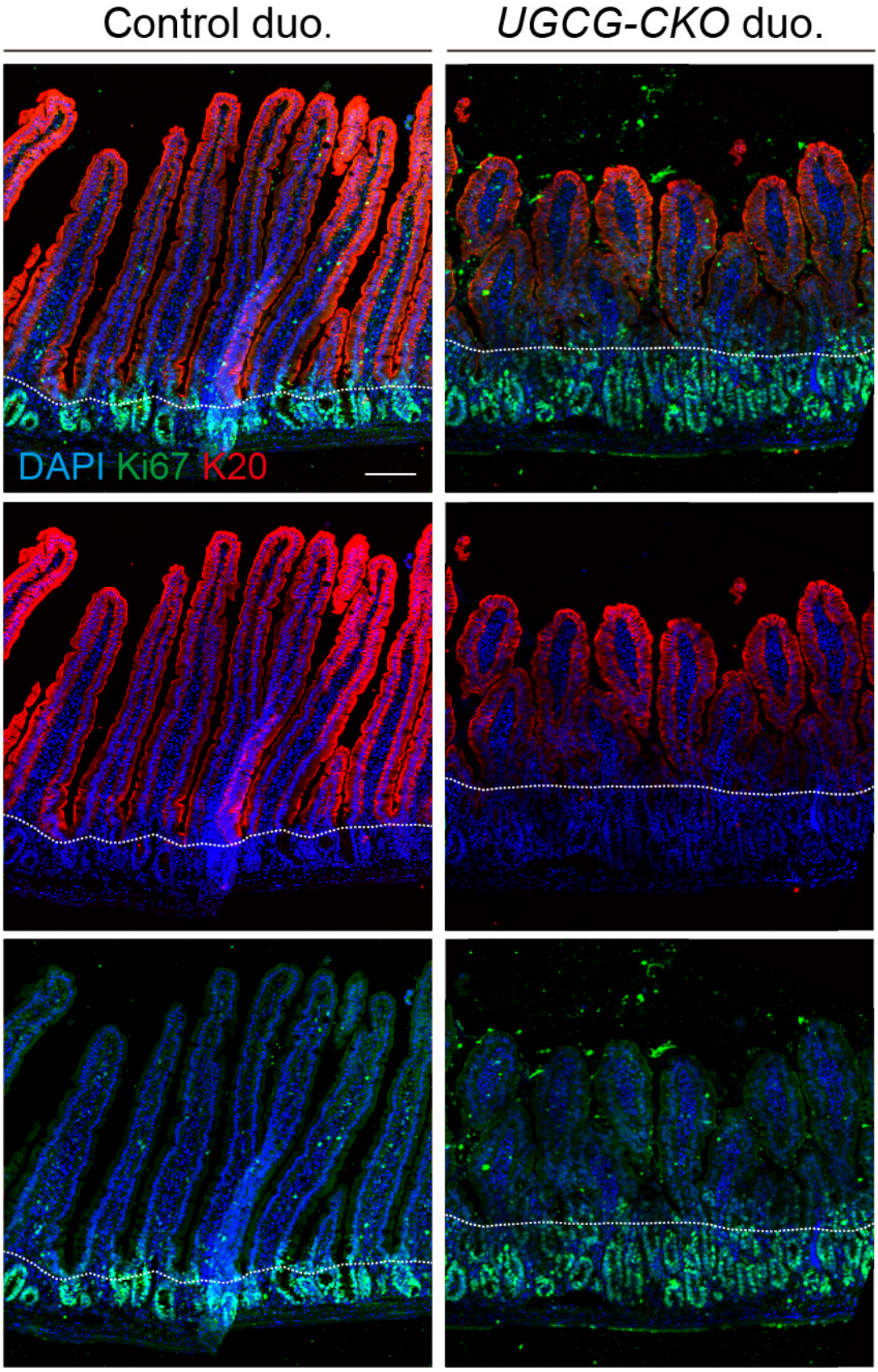
Control duo.
UGCG-CKO duo.
DAPI Ki67 K20

Supplementary Table 1. Summary of tumor suppression genes identified in the screen.

Gene/Label	Alleles identified	Function	Clone phenotype
mam	5	Mastermind (mam) encodes a transcriptional coactivator that functions in the Notch signaling pathway.	ISC and EE tumor*
Gmer	1	Gmer exhibits GDP-L-fucose synthase activity that are essential for fucosylation of Notch.	ISC and EE tumor
O-fut1	2	O-fut1 exhibits Notch binding activity and peptide-o-fucosyltransferase activity; positive regulation of Notch signaling pathway; and positive regulation of endocytosis.	ISC and EE tumor
GlcT (EA30, E230)	2	Glucosylceramide synthase (GlcT) encodes an enzyme that catalyzes the formation of glucosylceramide, the core component of glycosphingolipids.	ISC and EE tumor
n.d. (EA110)	1	n.d.	ISC and EE tumor
n.d. (EC230)	1	n.d.	ISC tumor**

n.d., not determined; * the mutant clones containing excessive numbers of ISCs, undifferentiated cells, and EEs; ** the mutant clones containing mainly ISCs.